NASA

Technical Memorandum 79721

Gravitational Spectra from the Tracking of Planetary Spacecraft in Eccentric Orbits

C. A. Wagner

MARCH 1979

National Aeronautics and
Space Administration

Goddard Space Flight Center
Greenbelt, Maryland 20771

TM 79721

GRAVITATIONAL SPECTRA FROM THE TRACKING OF PLANETARY SPACECRAFT IN ECCENTRIC ORBITS

C. A. Wagner
Geodynamics Branch
Goddard Space Flight Center
Greenbelt, MD 20771

March 1979

GODDARD SPACE FLIGHT CENTER
Greenbelt, Maryland

GRAVITATIONAL SPECTRA FROM THE TRACKING OF PLANETARY SPACECRAFT IN ECCENTRIC ORBITS

C. A. Wagner
Geodynamics Branch
Goddard Space Flight Center
Greenbelt, MD 20771

ABSTRACT

Two dimensional gravitational spectra are derived from simple harmonic analysis of range rate tracking data on planetary orbiters. The eccentricity of the orbit is arbitrary and results are shown to vary substantially with the aspect angle of the tracking line of sight with the orbit plane. The development for arbitrary start and stop times (with respect to periapsis) uses modified eccentricity functions evaluated by quadrature.

Simulations with a point–masses model of Venus using tracking data on the Pioneer Venus Orbiter show excellent predictions of the average orbiter spectrum over one Venus day. The Venus gravitational signal should be above the tracking noise level for arc lengths longer than 40° (in true anomaly) about periapsis and for terms as high as 55th degree.

Analysis has been made of tracking residuals from a short arc fit to Mariner Mars 9 data over the Hellas Basin (using a complete 6th degree field). Results are most consistent with higher residual gravitational power than predicted from Kaula's rule for Mars.

CONTENTS

ILLUSTRATIONS

ILLUSTRATIONS (Continued)

TABLES

GRAVITATIONAL SPECTRA FROM THE TRACKING OF PLANETARY SPACECRAFT IN ECCENTRIC ORBITS

INTRODUCTION

The spectrum of a surface harmonic field is a convenient summary of (roughly) the power available at a discrete seris of wavelengths. In the case of the gravitational field at the surface of a planet, the wavelength is also a fairly good indicator of the maximum depth of the equivalent spectrum of source anomalies (e.g., long wavelength, deep source, see Khan, 1977). Detailed interpretation of the spectrum in terms of the depth of density anomalies for the Earth began with Guier and Newton (1965) with notable analyses by Allan (1972), Lambeck (1976), and Kaula (1977). Recently Ferrari (1977) has applied Allan's method to the Moon and Mars. My purpose here is merely to show how easily the spectrum, in particular a smoothed version of it, can be derived directly from harmonic analysis of range rate tracking data to planetary orbiters. This work is an extension of the ideas in Wagner and Colombo (1978). Here I consider the 'fixed direction' tracking of spacecraft in eccentric orbits under arbitrary viewing angles with respect to the orbit plane and periapsis.

DEVELOPMENT OF THE TRACKING SPECTRUM

I define the spectrum of the planet's gravitational field as the potential degree variances:

$$\sigma_\ell^2 = \sum_{m=0}^{\ell} (\bar{C}_{\ell m}^2 + \bar{S}_{\ell m}^2),$$

where the external potential for a 'spherical' planet is given as

$$V = \frac{\mu}{r} \sum_{\ell=0}^{\infty} \sum_{m=0}^{\ell} \left(\frac{r_o}{r}\right)^\ell \bar{P}_{\ell m}(\sin\phi')[\bar{C}_{\ell m}\cos m\lambda' + \bar{S}_{\ell m}\sin m\lambda'],$$

r, ϕ', λ' being the distance from the center of mass, latitude and longitude respectively (r_o is the mean radius, μ the Gaussian gravity constant) and the $\bar{P}_{\ell m}$ are fully normalized associated Legendre functions (Heiskanen and Moritz, 1967). For convenience, I consider the planet to be without rotation and the surface spherical coordinate system to have a pole along the tracking

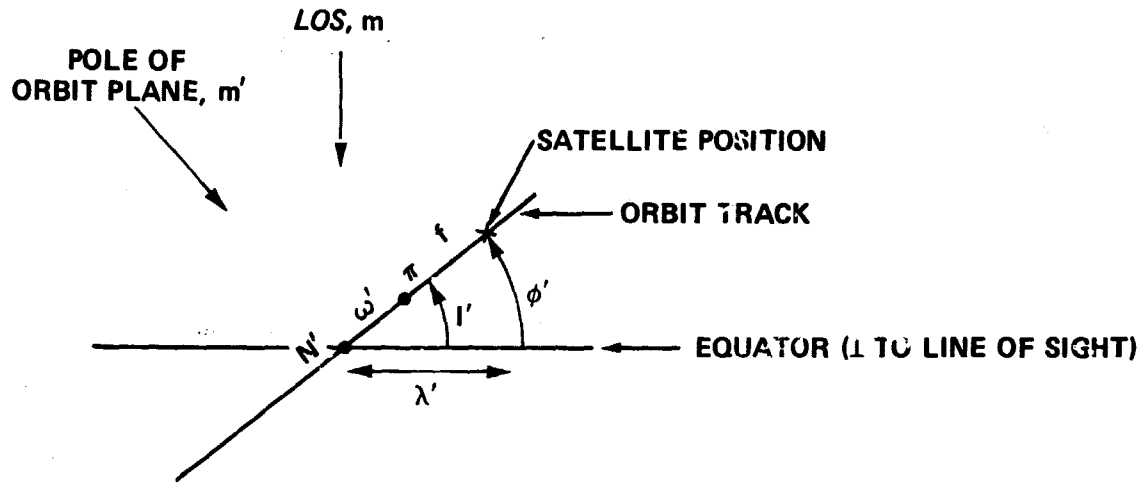

Figure 1. Coordinate System Orientations

Line of Sight (LOS). The field harmonics $V_{\ell m}$ are initially given in this system. But, we shall see that the invariance of the spectrum in rotation makes this initial choice arbitrary. In what follows, primed harmonics refer to the pole of the orbit plane: $(a', b')_{\ell m'}$. The periapsis of the orbit is at π and ω, f and I are the planet centered argument of periapsis, true anomaly and inclination of the orbit to the equator.

From Hotine (1969), the acceleration of the spacecraft by the gravitation field in the *LOS* direction is given in terms of fully normalized harmonics as:

$$\ddot{LOS} = \gamma \sum_{\ell=0}^{\infty} \sum_{m=0}^{\ell} \left(\frac{r_o}{r}\right)^{\ell+1} \bar{P}_{\ell m}(\sin\phi')[a_{\ell m}\cos m\lambda' + b_{\ell m}\sin m\lambda'] , \qquad (1)$$

where,

$$(a, b)_{\ell m} = N_{\ell m}(\bar{C}_{\ell-1,m}, \bar{S}_{\ell-1,m}) \text{ with}$$
$$N_{\ell m} = [(2\ell - 1)(\ell^2 - m^2)(2\ell + 1)^{-1}]^{1/2}, \text{ and} \qquad (2)$$
$$\gamma = \frac{\mu}{r_o^2}$$

To first order, the orbit of the spacecraft is an ellipse virtually unchanging in a single pass of the planet. Therefore, (to first order) we want to analyze a time series of the anomalous line of sight accelerations along the path of the fixed ellipse. This involves initially a transformation of the accelerations to a coordinate system with a pole normal to the orbit plane. Following Kaula (1966, p. 31, 34) (see also Wagner, 1976), I find:

$$LÖS = \gamma \sum_{\ell=0}^{\infty} \left(\frac{r_o}{r}\right)^{\ell+1} \sum_{m'=0}^{\ell(\ell-m' \text{ even})} \bar{P}_{\ell m'}(o)[a'_{\ell m'} \cos m'(\omega' + f) + b'_{\ell m'} \sin m'(\omega' + f)] , \qquad (3)$$

where

$$\bar{P}_{\ell m'}(o)\, a'_{\ell m'} = \sum_{m=0}^{\ell} [\bar{F}_{\ell,m,(\ell-m')/2}(I') + \bar{F}_{\ell,m,(\ell+m')/2}(I')] \begin{Bmatrix} a_{\ell m} \\ -b_{\ell m} \end{Bmatrix} \begin{matrix} \ell-m \text{ even} \\ \ell-m \text{ odd} \end{matrix} \qquad (4)$$

except

$$\bar{P}_{\ell o}(o)\, a'_{\ell o} = \sum_{m=0}^{\ell} \bar{F}_{\ell,m,\ell/2}(I') \begin{Bmatrix} a_{\ell m} \\ -b_{\ell m} \end{Bmatrix} \begin{matrix} \ell-m \text{ even} \\ \ell-m \text{ odd} \end{matrix} \quad \text{for } \ell \text{ even}, \qquad (5)$$

and

$$\bar{P}_{\ell m'}(o)\, b'_{\ell m'} = \sum_{m=0}^{\ell} [\bar{F}_{\ell,m,(\ell-m')/2}(I') - \bar{F}_{\ell,m,(\ell+m')/2}(I')] \begin{Bmatrix} b_{\ell m} \\ a_{\ell m} \end{Bmatrix} \begin{matrix} \ell-m \text{ even} \\ \ell-m \text{ odd} \end{matrix} . \qquad (6)$$

An efficient formula for evaluating the usual inclination functions $F_{\ell m p}(I')$ is found in Allan (1967a). Here the inclination functions, like the associated legendre functions, are fully normalized.

Finally, the anomalous accelerations can be written as a time series by expanding functions of r and f in terms of the mean anomaly (M) of the satellite in its orbit of semimajor axis 'a' and eccentricity 'e'. For a full revolution of data, using $[G_{\ell pq}(e)]$ Kaula's eccentricity functions (Kaula, 1966, p. 35), I find

$$\left(\frac{r_o}{r}\right)^{\ell+1} \begin{Bmatrix} \cos m'(\omega' + f) \\ \sin m'(\omega' + f) \end{Bmatrix} = \left(\frac{r_o}{a}\right)^{\ell+1} \sum_{n=0}^{\infty} \begin{Bmatrix} [\cos\omega' m'(G_+ + G_-)] \cos nm \\ [\sin\omega' m'(G_+ + G_-)] \cos nm \end{Bmatrix}$$
$$\begin{matrix} - [\sin\omega' m'(G_+ - G_-)] \sin nm \\ + [\cos\omega' m'(G_+ - G_-)] \sin nm \end{matrix} \Bigg\}, \qquad (7)$$

where

$$G_+ = G_{\ell,(\ell-m')/2,n-m'}(e),$$
$$G_- = G_{\ell,(\ell-m')/2,-n-m'}(e), \tag{8}$$

and the mean anomaly is a linear function of the time (t) from periapsis: $M = (2\pi/T)t$, T being the orbit period.

Let the periodic time series of accelerations for a full revolution be represented by the Fourier series:

$$\ddot{LOS} = \langle \ddot{LOS} \rangle + \sum_{n=1}^{\infty} (C\ddot{LOS}_n \cos n m + S\ddot{LOS}_n \sin n m) \tag{9}$$

Then Equations (7), (6), (5) and (4) substituted in (3) gives the Fourier Coefficients of Equation (9) as

$$C\ddot{LOS}_n = \gamma \sum_{\ell=0}^{\infty} \left(\frac{r_o}{a}\right)^{\ell+1} \sum_{m'=0}^{\ell(\ell-m' \text{ even})} \cos\omega' m' [G_+ + G_-] \sum_{m=0}^{\ell} [\bar{F}_- + \bar{F}_+] \begin{Bmatrix} a_{\ell m} \\ -b_{\ell m} \end{Bmatrix} \begin{matrix} \ell-m \text{ even} \\ \ell-m \text{ odd} \end{matrix}$$
$$+ \sin\omega' m' [G_+ + G_-] \sum_{m=0}^{\ell} [\bar{F}_- - \bar{F}_+] \begin{Bmatrix} b_{\ell m} \\ a_{\ell m} \end{Bmatrix} \begin{matrix} \ell-m \text{ even} \\ \ell-m \text{ odd} \end{matrix}, \tag{10}$$

and

$$S\ddot{LOS}_n = \gamma \sum_{\ell=0}^{\infty} \left(\frac{r_o}{a}\right)^{\ell+1} \sum_{m'=0}^{\ell(\ell-m' \text{ even})} - \sin\omega' m' [G_+ - G_-] \sum_{m=0}^{\ell} [\bar{F}_- + \bar{F}_+] \begin{Bmatrix} a_{\ell m} \\ -b_{\ell m} \end{Bmatrix} \begin{matrix} \ell-m \text{ even} \\ \ell-m \text{ odd} \end{matrix}$$
$$+ \cos\omega' m' [G_+ - G_-] \sum_{m=0}^{\ell} [\bar{F}_- - \bar{F}_+] \begin{Bmatrix} b_{\ell m} \\ a_{\ell m} \end{Bmatrix} \begin{matrix} \ell-m \text{ even} \\ \ell-m \text{ odd} \end{matrix}, \tag{11}$$

where

$$\bar{F}_- = \bar{F}_{\ell,m,(\ell-m')/2}(I'),$$
$$\bar{F}_+ = \bar{F}_{\ell,m,(\ell+m')/2}(I'),$$

except that if $m' = 0$, only one $\bar{F}$ is used in $[\bar{F}_- + \bar{F}_+]$.

Let the power spectrum of these accelerations be:

$$P_n^2(L\ddot{O}S) = \frac{1}{2}\left[CLOS_n^2 + SLOS_n^2\right].$$

What is the expected power spectrum over all possible *LOS* positions with respect to the planet (I', ω' constant)? I have no answer to this question at present. But there is an easy answer to a complementary ergodic question and that answer appears to be the same. The complementary question is: What is the expected spectrum for a given *LOS* position over all possible gravitational fields $[\bar{C}^*, \bar{S}^*]$ whose potential coefficients are chosen randomly, in an uncorrelated manner with:

$$E(\bar{C}_{\ell m}^{*2}, \bar{S}_{\ell m}^{*2}) = \delta_\ell^2,$$

where,

$$\delta_\ell^2 = \sigma_\ell^2 / (2\ell + 1),$$

the mean square coefficient of the planet's field by degree?

Squaring Equations (10) and (11) [written for the random field (a^*, b^*)], and taking the expectations (noting that the expectations of cross products of field coefficients are zero), the result is:

$$E[P_n^2(L\ddot{O}S)] = \gamma^2 \sum_{\ell=0}^{\infty} \left(\frac{r_o}{a}\right)^{2(\ell+1)} \delta_{\ell-1}^2 \sum_{m'=0}^{\ell(\ell-m' \text{ even})} \left\{ (G_+^2 + G_-^2) \sum_{m=0}^{\ell} (\bar{F}_-^2 + \bar{F}_+'^2) N_{\ell m}^2 \right.$$
$$\left. + 4(\cos 2\omega' m') G_+ G_- \sum_{m=0}^{\ell} \bar{F}_- \bar{F}_+' N_{\ell m}^2 \right\}, \tag{12}$$

where:

$$\bar{F}_+' = \bar{F}_+, \quad m' \neq 0$$
$$\bar{F}_+' = 0, \quad m' = 0$$

Note the dependence of this result on the gravitational spectrum (δ_ℓ^2). While the reference for the field is along the *LOS*, the surface spectrum is the same with respect to any pole. In particular, the $\delta_{\ell-1}^2$ in Equation (12) are the same as the field spectrum conventionally referred to the planet's North Pole.

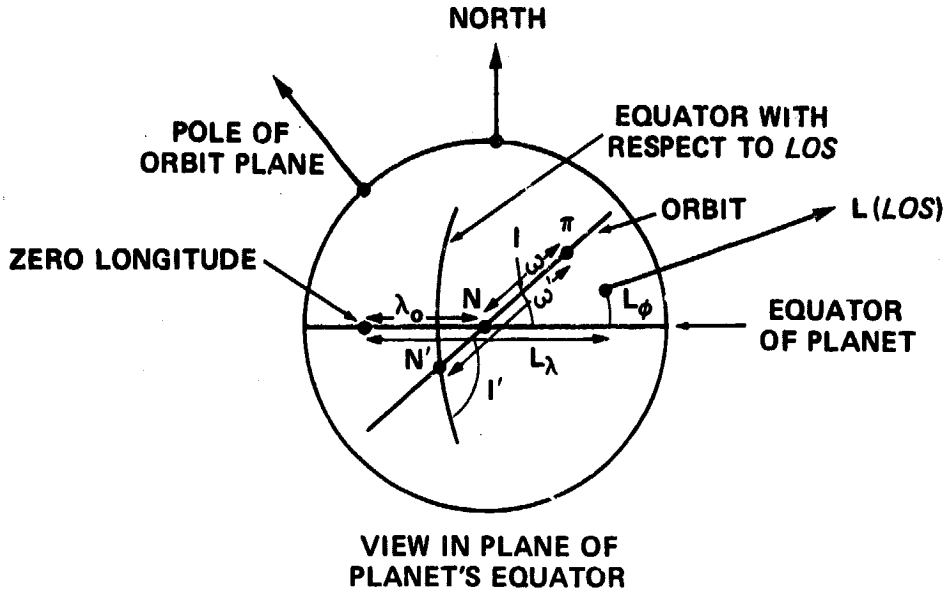

Figure 2. Planet, Orbit and *LOS* Coordinates

To utilize Equation (12) for predicting the tracking spectrum, we need to find I′ and ω' (the complements of the aspect angles of the view (L) with respect to the orbit plane and the periapsis direction) in terms of conventional planet centered coordinates (Fig. 2). Using Figure 2, I find:

$$I' = \cos^{-1}[\cos I \sin L_\phi + \sin I \cos L_\phi \sin(\lambda_o - L_\lambda)], \tag{13}$$

and

$$\omega' = 90^\circ - \cos^{-1}\left\{[\sin\pi_\phi \sin L_\phi + \cos\pi_\phi \cos L_\phi \cos(L_\lambda - \pi_\lambda)]/\sin I'\right\}, \tag{14}$$

where π_ϕ, π_λ are the planet centered latitude and longitude of periapsis, L_ϕ, L_λ are the corresponding coordinates of the viewing direction (*LOS*) and λ_o is the planet centered longitude of the ascending equator crossing of the orbit.

The expected spectrum for given aspect angles of the view can be simplified for average or more specific viewing conditions. From (12) the expected spectrum averaged over all aspect angles ($90^\circ - \omega'$) with respect to periapsis is simply

$$E[P_n^2(L\ddot{O}S)]_{\langle\omega'\rangle} = \gamma^2 \sum_{\ell=0}^{\infty} \left(\frac{r_c}{a}\right)^{2(\ell+1)} \delta_{\ell-1}^2 \sum_{m'=0}^{\ell(\ell-m' \text{ even})} (G_+^2 + G_-^2) \sum_{m=0}^{\ell} (\overline{F}_-^2 + \overline{F}_+'^2) N_{\ell m}^2 . \tag{15}$$

Calculations show the periapsis aspect has little affect on the average spectrum when full realistic fields are considered. However, the spectrum changes by over 100% with viewing aspect to the orbit plane (90°-I'). Maximum power occurs when viewing in the orbit plane, minimum when the *LOS* is normal to the plane. This spectrum for the Cross Track (CT) view is especially simple to find since for I' = 0, the only non zero $\bar{F}$ is (from Allan, 1967b, p. 1836):

$$\bar{F}_{\ell,m',(\ell-m')/2}(o) = \bar{P}_{\ell m'}(o),$$

so that:

$$E[P_n^2(\ddot{CT})]_{\langle\omega'\rangle} = \gamma^2 \sum_{\ell=0}^{\infty} \left(\frac{r_o}{a}\right)^{2(\ell+1)} \delta_{\ell-1}^2 \sum_{m'=0}^{\ell(\ell-m' \text{ even})} (G_+^2 + G_-^2)\bar{P}_{\ell m'}^2(o)N_{\ell m'}^2, \qquad (16)$$

a generalization of the result for circular orbits in Wagner and Colombo (1978, p. 6).

The expected spectrum, averaged again over all viewing aspects (I') can be estimated from the invariance (Wagner, 1977):

$$\sum_{m=0}^{\ell} (\bar{F}_-^2 + \bar{F}_+^2) \equiv \bar{P}_{\ell m'}^2(o).$$

Thus in Equation (15), the averaged spectrum is estimated to carry a constant averaged $N_{\ell m}^2$:

$$\bar{N}_{\ell m}^2 = (2\ell+1)^{-1} \sum_{m=0}^{\ell} N_{\ell m}^2 = \frac{\ell(2\ell-1)^2}{3(2\ell+1)},$$

so that:

$$E[P_n^2(\ddot{LOS})]_{\langle\omega',I'\rangle} = \gamma^2 \sum_{\ell=0}^{\infty} \left(\frac{r_o}{a}\right)^{2(\ell+1)} \delta_{\ell-1}^2 \left(\frac{\ell(2\ell-1)^2}{3(2\ell+1)}\right) \sum_{m'=0}^{\ell(\ell-m' \text{ even})} (G_+^2 + G_-^2)\bar{P}_{\ell m'}^2(o), \qquad (17)$$

a similar generalization of the result in Wagner and Colombo (1978, p. 6).

In general, the anomalous gravitational power spectrum on eccentric orbits contain effects at all frequencies from every gravitational term. Here power from a term of degree $\ell-1$ radiates to frequencies n greater than ℓ as well as n less than ℓ. However, as will be seen, except for low degree terms, most of the radiation of power is still downwards.

THE POWER SPECTRUM FOR INCOMPLETE ARCS OF DATA

The track spectrum for data from circular orbits tends to be uniform over the span of the arc. The anomalous accelerations are everywhere at the same distance from the planet. In an eccentric orbit, however, the accelerations are smaller away from periapsis, distorting the spectrum. This distortion is accounted for by the development for a full revolution of data with the Kaula eccentricity functions [Equation (7)]. But, for the partial arcs of tracking data which are actually taken, these results cannot be used directly.

One solution to this problem would be to complete a full revolution with artificial data in a reasonable manner. A more straightforward approach is to develop the spectrum for data over arcs less than a full revolution. For this purpose consider an orbit function defined on the interval M_{min} to M_{max} (Fig. 3).

The objective functions and their expansions [see Equation (7)] are of the form:

$$H(M) = (r/a)^u \exp(ivf) = \sum_{n=-\infty}^{\infty} X_n'^{u,v}(e)\exp(inM'). \qquad (18)$$

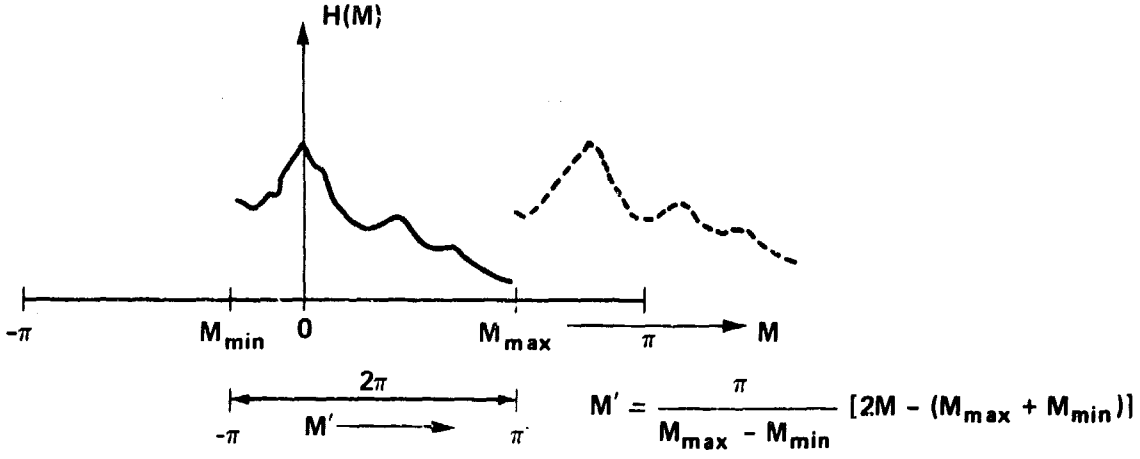

Figure 3. Development Interval for Orbit Functions

Here, u and v are integers ($i = \sqrt{-1}$) and n are the frequencies (or wave numbers) of the Fourier expansion in the interval $-\pi$ to π of the modified mean anomaly M'. The notation for the Fourier coefficients follows that for the Hansen coefficients which develop the orbit functions for full revolutions (e.g., Allan, 1967b, p. 1843, 1844).

To evaluate these modified or partial Hansen coefficients, multiply both sides of (18) by one particular wave, exp (-inM'), and integrate with respect to M' from $-\pi$ to π. Only the particular wave term remains, yielding:

$$X_n'^{u,v}(e) = \frac{1}{2\pi} \int_{-\pi}^{\pi} (r/a)^u \exp i(vf - nM')\, dM'. \tag{19}$$

In general, $M_{max} \neq |M_{min}|$ and $vf - nM'$ is not an odd function about $M' = 0$. Thus, for an unevenly sampled arc about periapsis, the modified Hansen coefficients are complex numbers:

$$\mathcal{R}X_n'^{u,v}(e) = \frac{1}{2\pi} \int_{-\pi}^{\pi} (r/a)^u \cos(vf - nM')\, dM' \tag{20}$$

$$\mathcal{I}X_n'^{u,v}(e) = \frac{1}{2\pi} \int_{-\pi}^{\pi} (r/a)^u \sin(vf - nM')\, dM', \tag{21}$$

and the spectrum of the orbit functions contain twice as many terms as in Equation (7). But since most of the useful data on high eccentricity orbits will be fairly close to periapsis on both sides, it is convenient to study the simpler case of even sampling centered on periapsis. In this case, the modified Hansen coefficients are real only [Equation (20)] as they are for full revolutions. The development in Equation (7) is then the same with the use of modified Kaula functions $G'_{\ell pq}(e)$ where

$$G'_{\ell pq}(e) = X'^{-\ell-1,\ell-2p}_{\ell-2p+q}(e) = \frac{1}{2\pi} \int_{-\pi}^{\pi} (a/r)^{\ell+1} \cos[(\ell - 2p)f - (\ell - 2p + q)M']\, dM', \tag{22}$$

and

$$M' = \pi M/M_{max}.$$

The modified G functions have been evaluated to high eccentricity, with reasonable speed, directly from their integral definition in (22). To facilitate quadratures which depend on equal argument steps and to avoid the solution of Kepler's equation at each step, it is convenient to change the argument in (22) to eccentric anomaly:

$$G_{\ell pq}(e) = \frac{1}{M_{max}} \int_0^{E_{max}} (1 - e\cos E)^{-2} \cos\left\{2(\ell - 2p)\,\mathrm{Tan}^{-1}\left[\sqrt{(1+e)/(1-e)}\,\right]^{1/2} \cdot \mathrm{Tan}\,E/2\right] - \frac{\pi}{M_{max}}(\ell - 2p + q)(E - e\sin E)\right\} dE, \tag{23}$$

where

$$M_{max} = E_{max} - e\sin E_{max}.$$

SIMULATIONS

Numerous calculations have been made with harmonic and point-mass Earth models which verify the track spectrum predicted for the eccentric orbiter. In these analyses, the anomalous *LOS* accelerations along a fixed ellipse are integrated numerically over a given arc length T_A in time.

Imagine a set of *LOS* acceleration data given in this arc. The harmonic analysis of this data yields the coefficients in the expansion:

$$L\ddot{O}S = L\ddot{O}S_0 + \sum_{n=1}^{\infty} (CL\ddot{O}S_n \cos 2\pi nt/T_A + SL\ddot{O}S_n \sin 2\pi nt/T_A). \tag{24}$$

Integrating (24), the *LOS* velocities (or range rates) are:

$$L\dot{O}S = L\dot{O}S_0 + L\ddot{O}S_0 t + \sum_{n=1}^{\infty} (T_A/2\pi n)\, CL\ddot{O}S_n \sin 2\pi nt/T_A - (T_A/2\pi n)\, SL\ddot{O}S_n \cos 2\pi nt/T_A. \tag{25}$$

The secular term $L\ddot{O}S_0 t$ can be eliminated by subtracting from the velocities a trend line connecting the first and last points ($t = 0, T_A$), which also guarantees continuity of the data there. The

power spectrum of the resulting (*LOS*) velocity data ($n>0$) is then related to the power spectrum of the source accelerations by:

$$P_n^2(L\ddot{O}S) = (2\pi n/T_A)^2 P_n^2(L\dot{O}S), \tag{26}$$

which also holds for expectations.

The point-masses (Mascon) model investigated consisted of the central mass (μ) of the Earth with 266 randomly chosen concentrations in three layers. The mass magnitudes and locations in the shallowest layer (20km depth) are shown in Figure 4 (units: $1.8 \times 10^{-6}\mu$). The locations of the masses in the 2 deeper layers are also shown (see also, Wagner and Colombo, 1978, p. 16). The gravitational spectrum of this model (Fig. 5) is somewhat weaker than Kaula's rule for the Earth (Kaula, 1966, p. 98).

The fidelity of the spectrum predicted for this model is best revealed in analyses of the fundamental *LOS* anomalous accelerations themselves. Twenty orbit-arcs were generated with random inclinations and nodes for the same (Pioneer-Venus) orbit shape (perigee height: 200km, eccentricity 0.844, period: 24 hours). Periapsis locations and (infinite distance) viewing aspects (I', ω') were also chosen randomly (Fig. 6). All arcs were 180° long in true anomaly (52 minutes) centered at periapsis. (The planet did not rotate during the arc.)

For an extreme example, the *LOS* accelerations in arc 1, with periapsis directly over a fairly strong near-surface concentration, is shown in Figure 7. The power spectrum for this arc (Fig. 8) is deficient at low frequencies. The expected spectrum has been calculated for average viewing aspects from Equation (17). It gives good predictions for higher frequencies, anticipating the presence of some 'spikey' behaviour in a typical arc over this model.

The harmonic analyses of accelerations were done without matching the end points, to conform with the development of the accelerations over a partial revolution. As Figure 9 shows, the average power spectrum for the 20 arcs is remarkably well predicted by the theory, even to the highest frequencies dominated by the effect of the discontinuity at the end points.

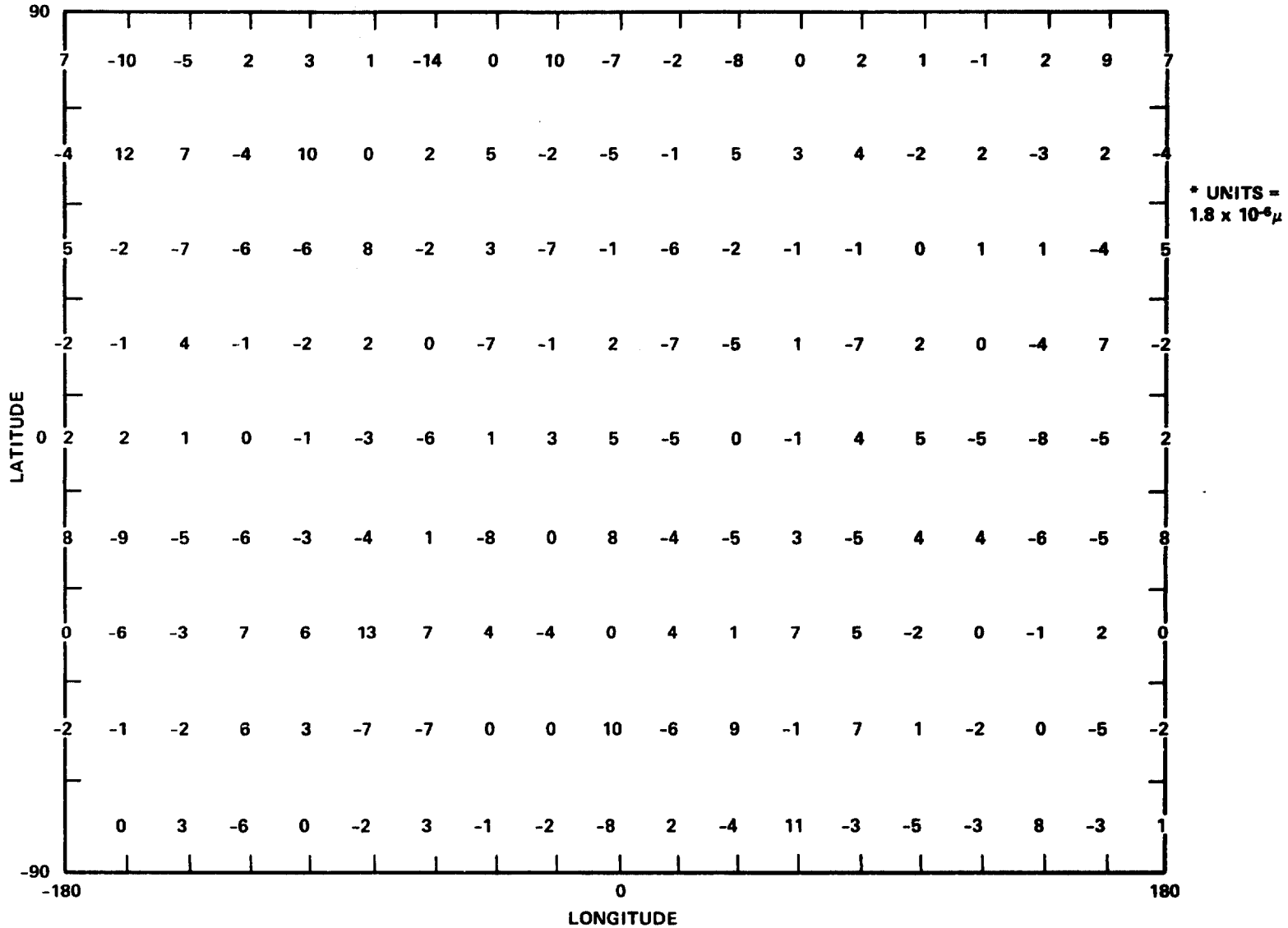

Figure 4. Point Mass Magnitudes at 20km Depth for Model Planet*

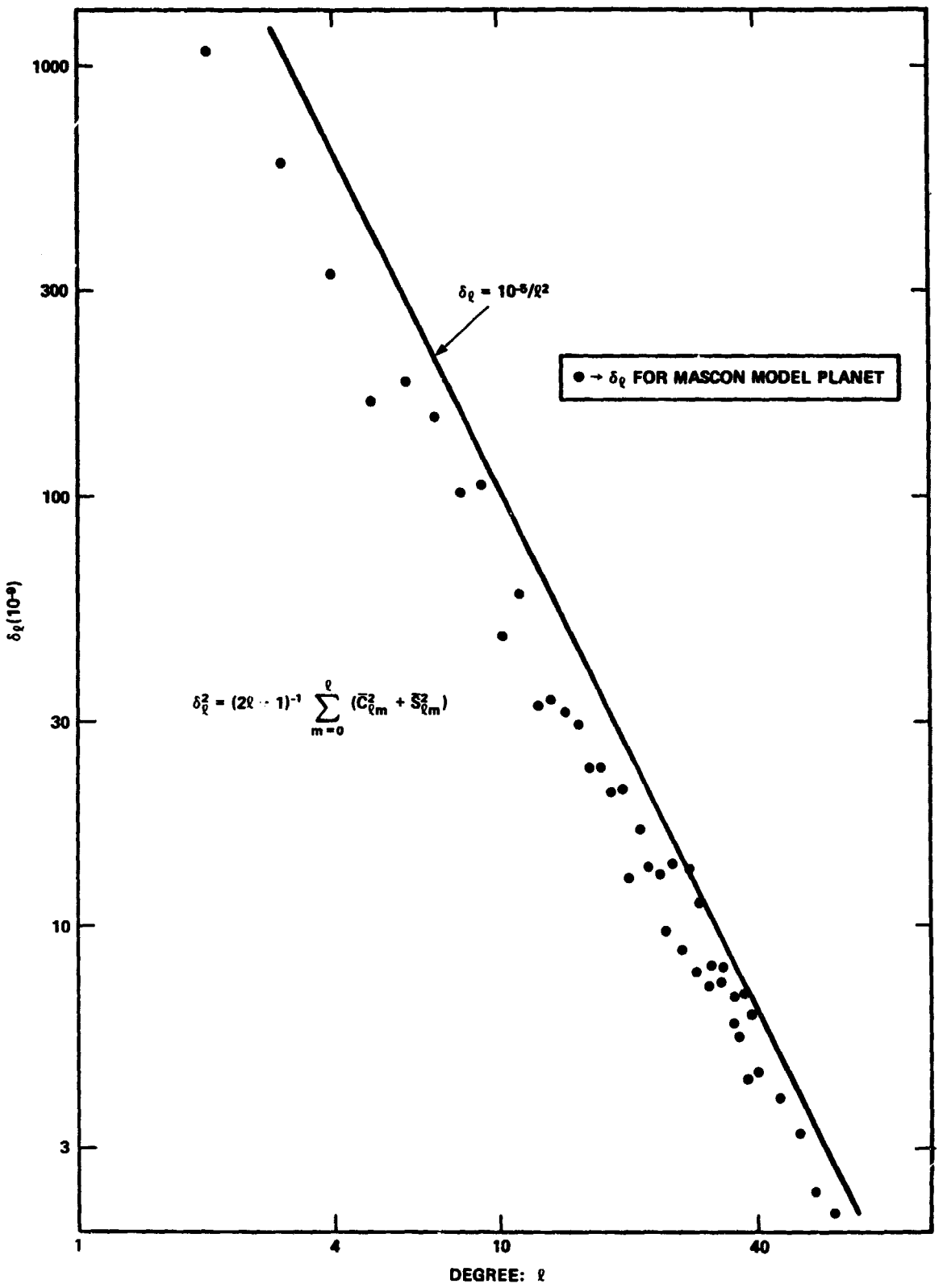

Figure 5. Gravitational Spectra

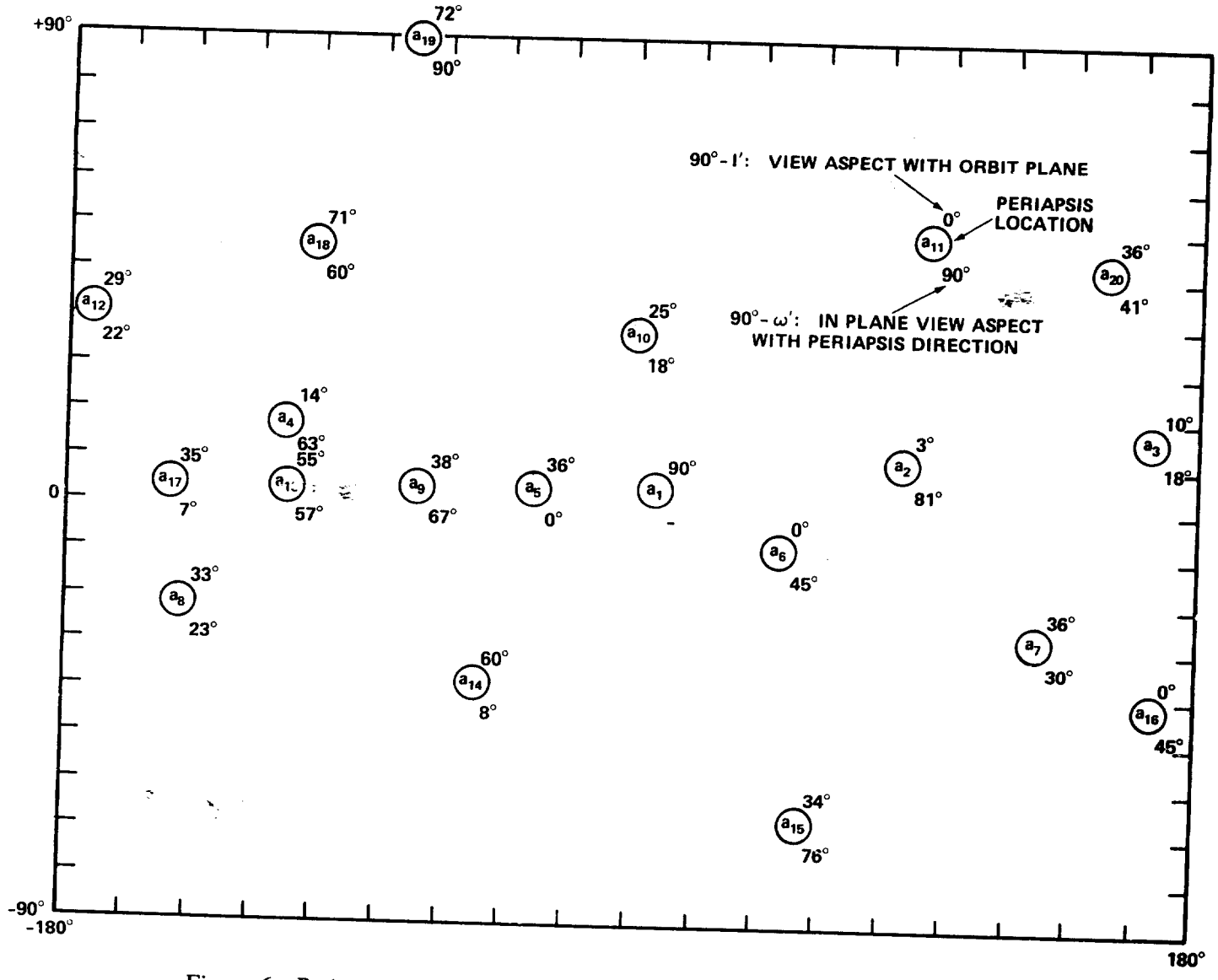

Figure 6. Periapsis Locations and View Aspects for 20 Acceleration-Data Arcs

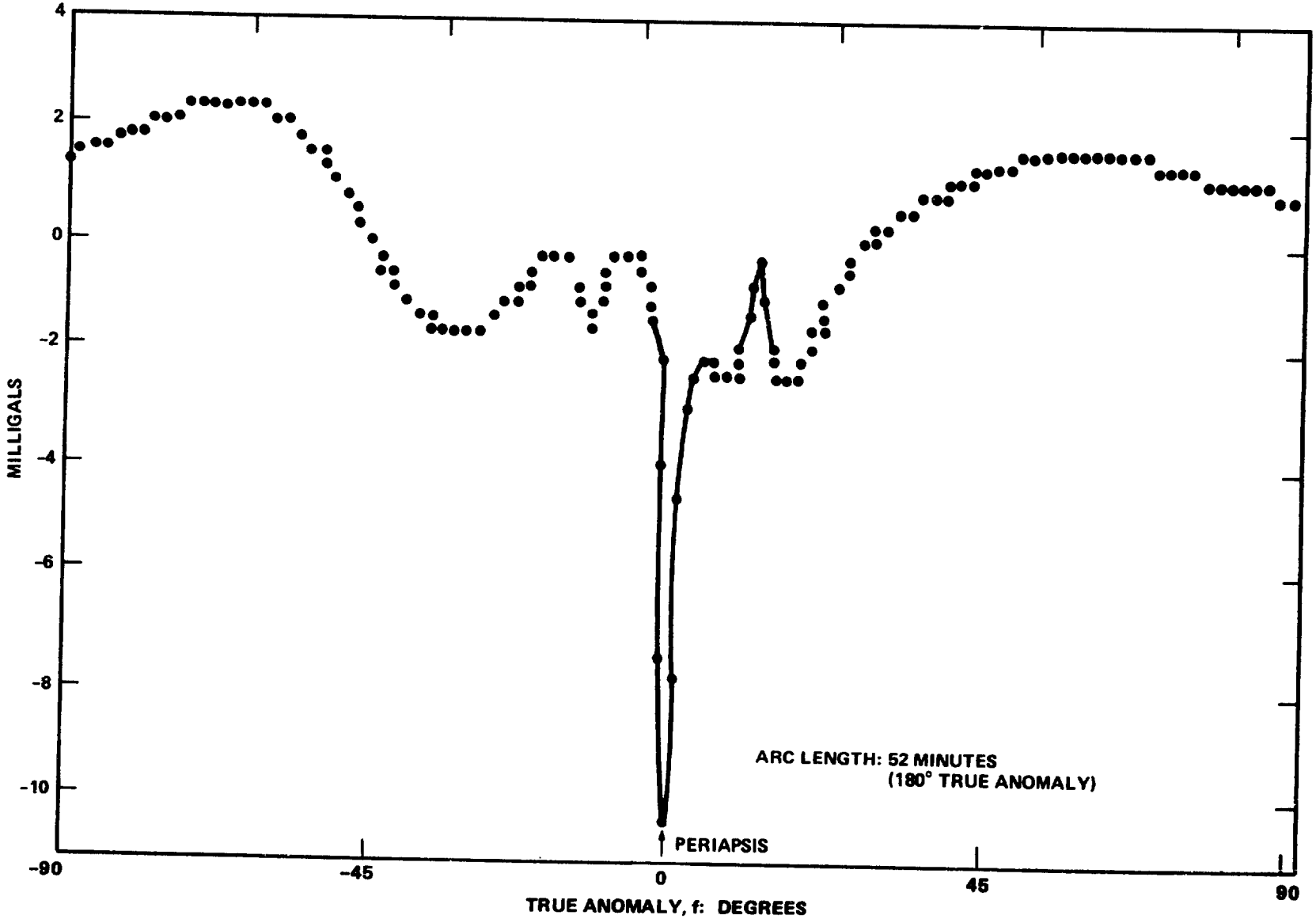

Figure 7. Anomalous Line of Sight Acceleration – Arc 1

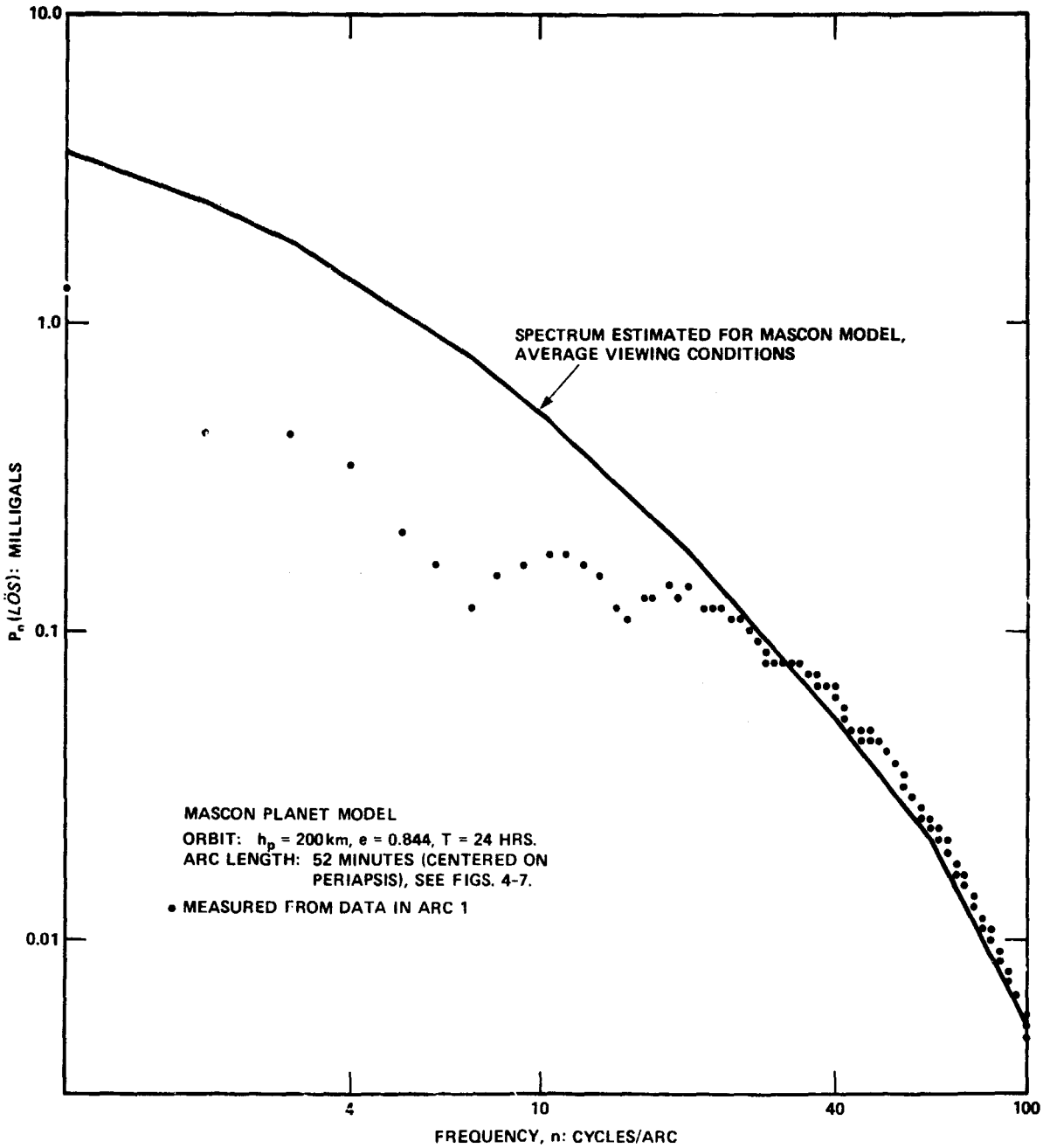

Figure 8. Power Spectrum of Simulated Anomalous *LOS* Accelerations – Arc 1

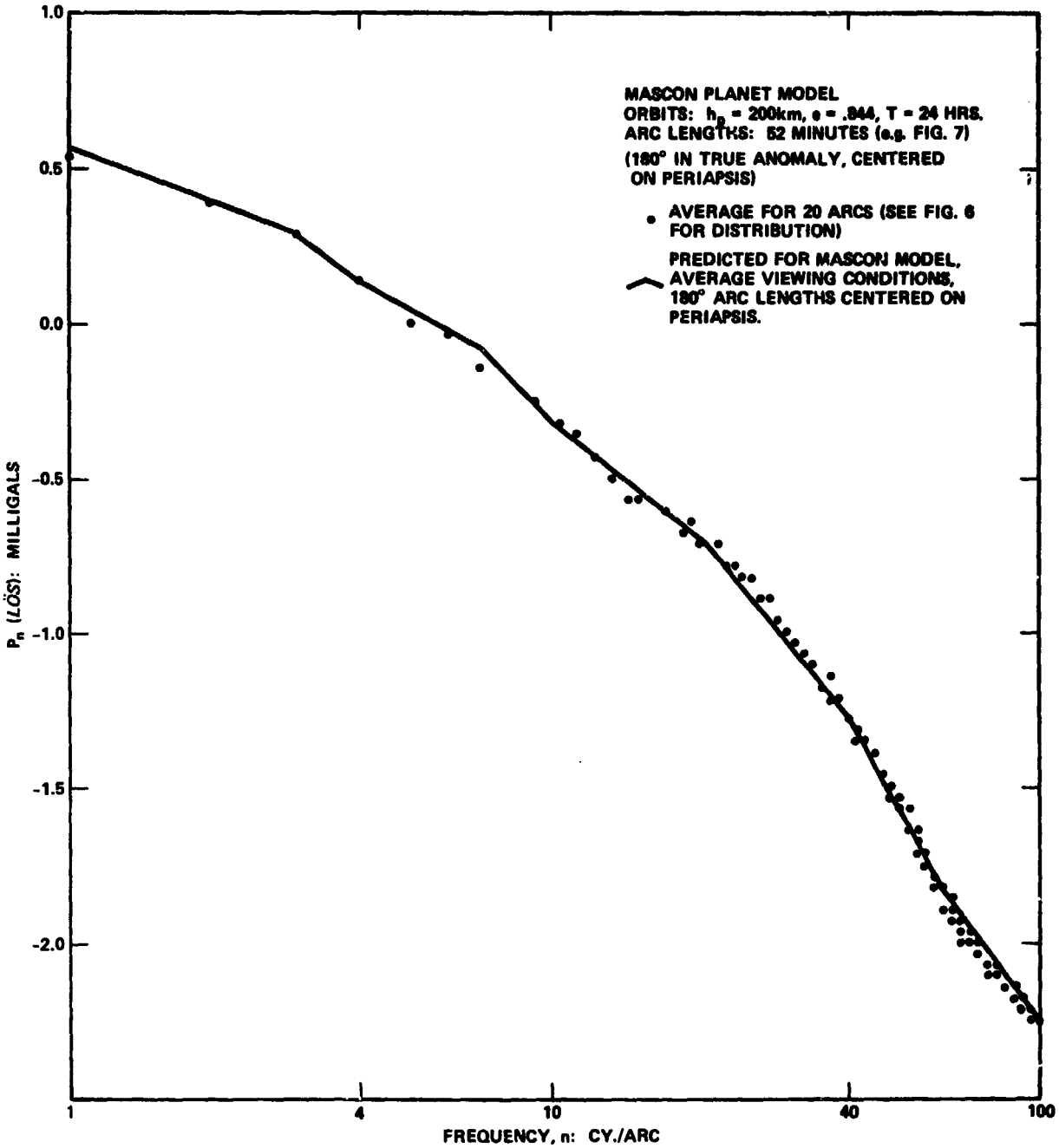

Figure 9. Average Power Spectrum for 20 *LOS* Acceleration-Data Arcs

The analysis of velocity or *LOS* range rate perturbations requires the data at the ends of the arc to be matched. When this is done, predictions of the spectrum are excellent. For example, 40 similar (180° periapsis centered) arcs of *LOS* range rate perturbations were analyzed. Here, periapsis locations were random, but all views were in that direction. The planet model in this case, however, was a simple harmonic one consisting of just the complete (0,0) through (2,2) terms of the Mascon field. Orbit and spectrum computations for this truncated model were considerably faster than with the full field. Also, it was felt the average arc results would converge faster on the expected spectrum since severe distortions at periapsis would be avoided (as in arc a_1).

Actually, it appears to take more arcs to determine a good average spectrum for just these low harmonics than for the whole field. Limited local sampling is a notoriously poor way to determine global low order harmonics or their average effects. Nevertheless, the results of these analyses, with all views in the direction of periapsis, afforded a good test of the predictions for various aspect angles. The spectrum from low order terms shows considerably more power with along track viewing at periapsis than at any other aspect. The results (in Fig. 10) confirm the validity of the aspect dependent parts of the theory [calculated from Equations (12) and (26)]. It also shows the considerable amount of power radiated (in an eccentric orbit) to frequencies (n) higher than the maximum field degree (ℓ).

In the circular orbit case there is no such power radiated upwards except that due to the end discontinuity. This latter effect can be minimized by matching higher derivitives (Wagner and Colombo, 1978, p. 8, 18). But this adjustment is no longer needed with the present, more general theory for partial revolution data which predicts this high frequency 'ramp' distortion.

SIMULATION OF PIONEER VENUS ORBITER MISSION

In an illustration of results which should be forthcoming from the Pioneer-Venus mission, I have analyzed the anomalous *LOS* velocity residuals in 10 partial revolution arcs over the Mascon model planet. The coverage of this data is shown within the dashed lines of Figure 11. Notice

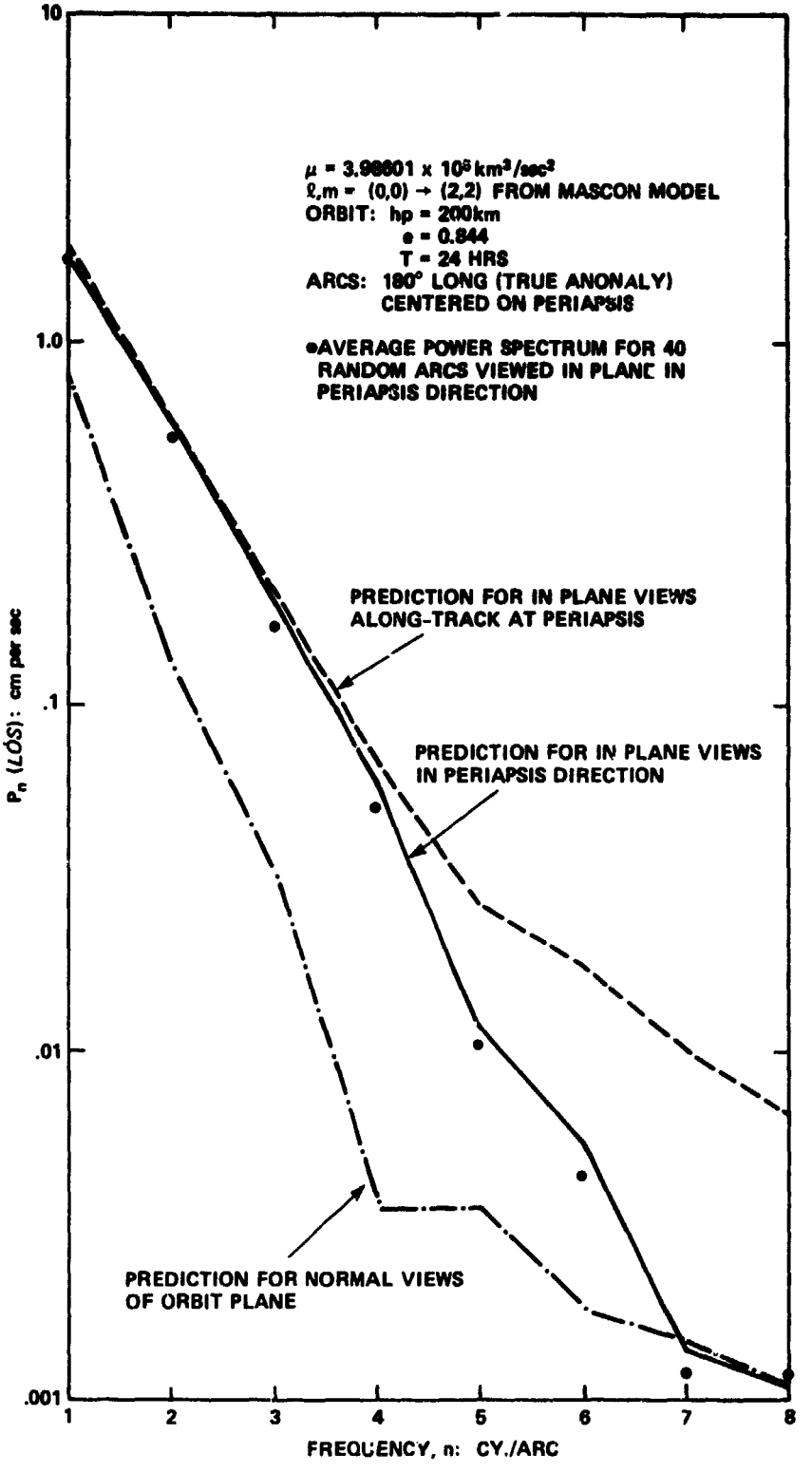

Figure 10. Track Power Spectra for a Low Order Gravitational Field Model

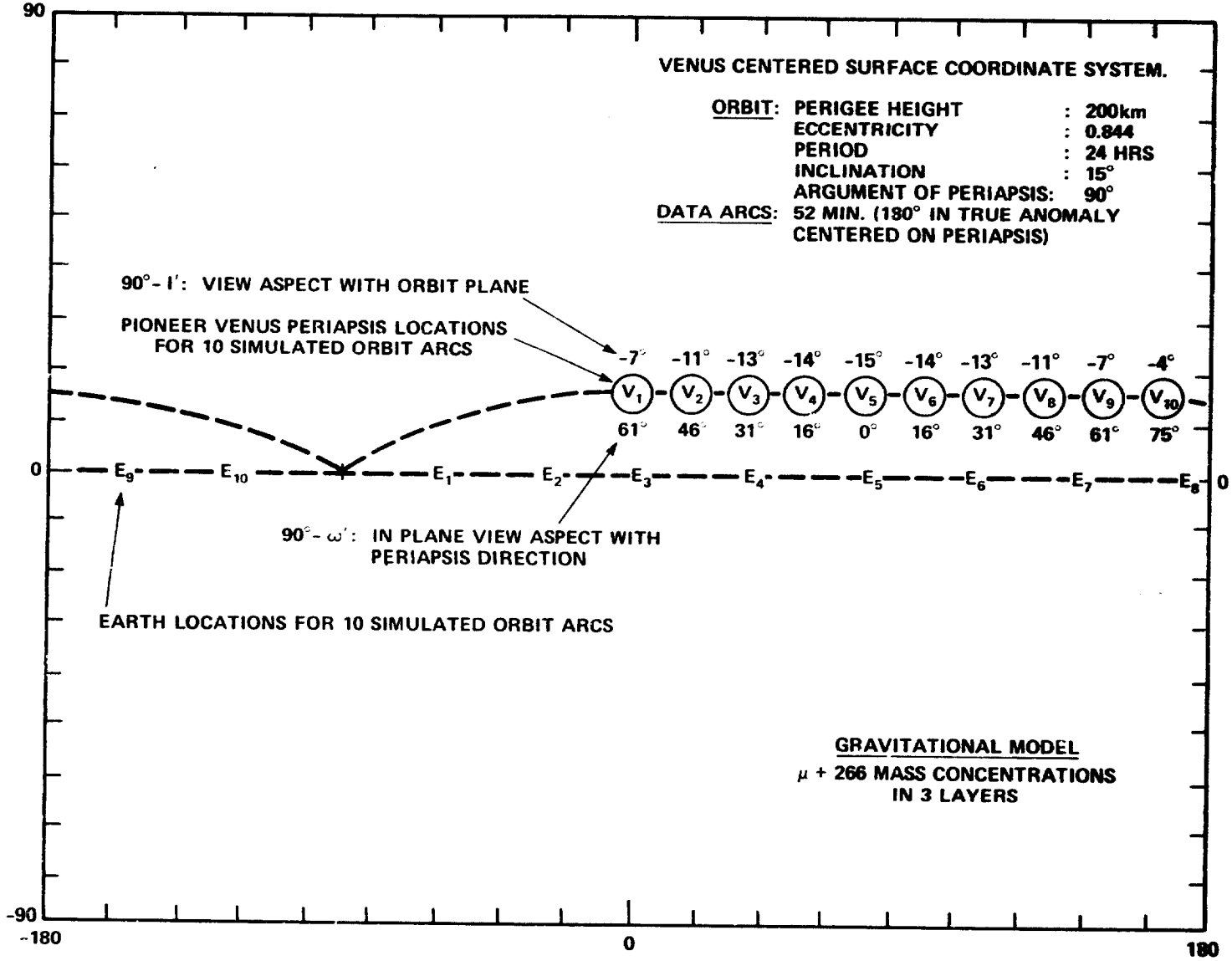

Figure 11. Periapsis and Earth Locations in 120-Day Pioneer Venus Mission

that only a narrow band north of the equator is covered and the viewing aspect to the orbit plane is also limited. But the average spectrum for these arcs is still fairly well predicted (using average viewing conditions) as seen in Figure 12.

More detailed estimations for Pioneer Venus have been made with a smooth power spectrum of the form:

$$\delta_\ell = A\ell^B .$$

Here B = −2 as in Kaula's rule for the Earth and A is scaled (from 1 x 10^{-5} for the Earth) to the size and masses of the terrestrial planets such that interior stresses are the same as in the Earth (Kaula, 1969). Thus, for Mars and the Moon, A should be 6.76 x 10^{-5} and 36.45 x 10^{-5}; in fair agreement with the actual low degree field (Gapcynski, Tolson, and Michael, 1977; Ananda, 1977). The scale rule is:

$$\frac{A(\text{Terr. Planet})}{10^{-5}} = \left(\frac{\mu_e}{\mu_p}\right)^2 \left(\frac{r_p}{r_e}\right)^4 ,$$

so that for Venus it is estimated that A = 1.22 x 10^{-5}.

Using this smooth spectrum and the elements for Pioneer Venus: Perigee height 200 km, period 24 hours (eccentricity: 0.844), I have calculated the expected spectrum for two (typical) data arcs centered on periapsis (Figs. 13a and 13b). The upper bound line (for average views) includes effects of 1st degree harmonics which may be removed with better knowledge of the position of the center of mass of Venus. Notice in Figure 13a the large variation (up to 200%) of expected power with the orbit plane viewing aspect. The variation over periapsis aspects (for the full field) is much less significant. These figures can be used to estimate the spectrum of the field not included in the orbital data reduction, i.e., the truncation power.

For example, if the 2-way Doppler range rate data has an intrinsic accuracy of 0.03 cm/sec for an averaging interval of 1 minute and 26 frequencies are estimated in the 180° (52 minute) arc then the 'white' noise level for each frequency will be $0.03/(26)^{1/2}$ = 0.006 cm/sec/frequency.

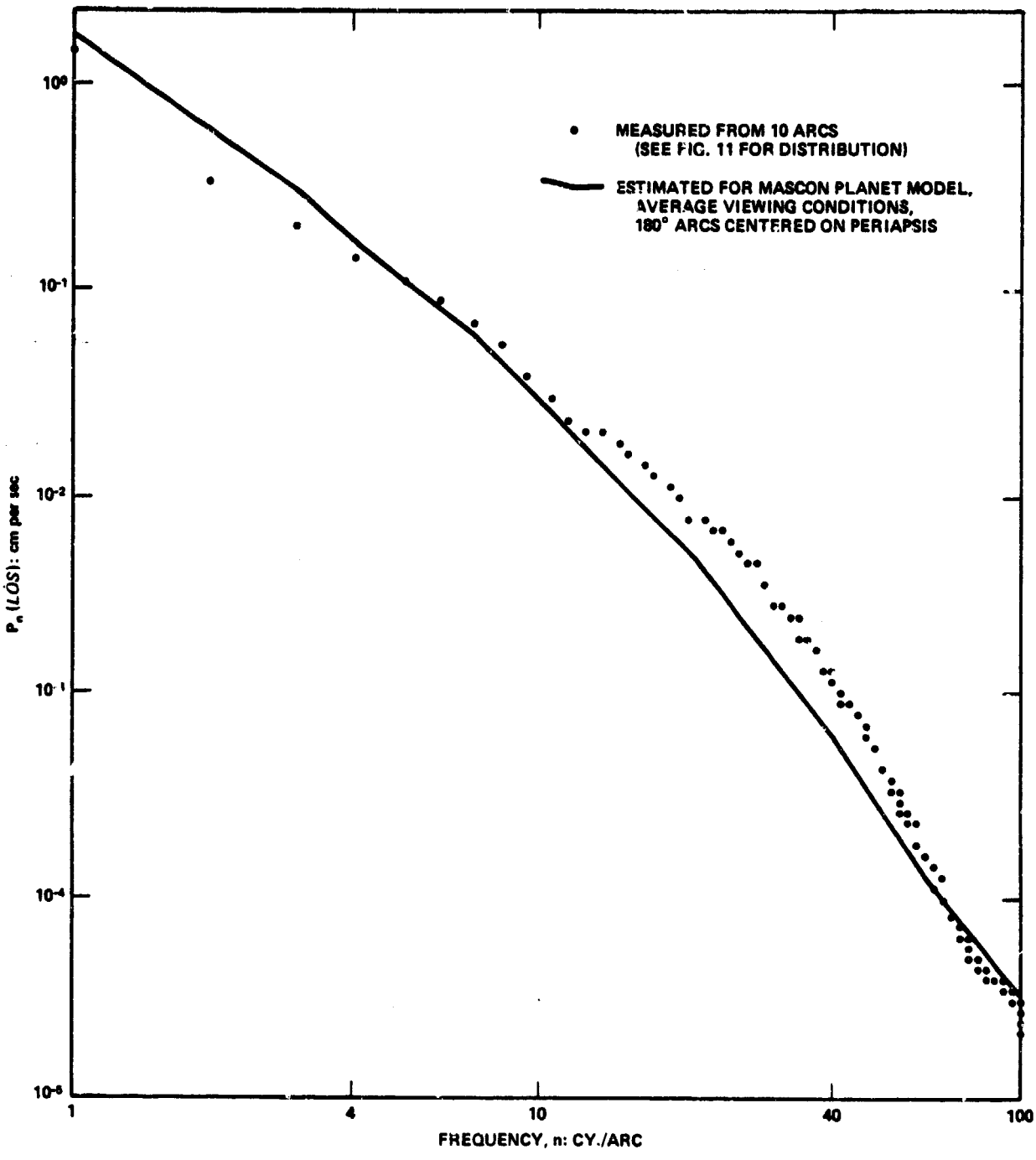

Figure 12. Average Range Rate Power Spectrum from 120-Day Pioneer Venus Mission

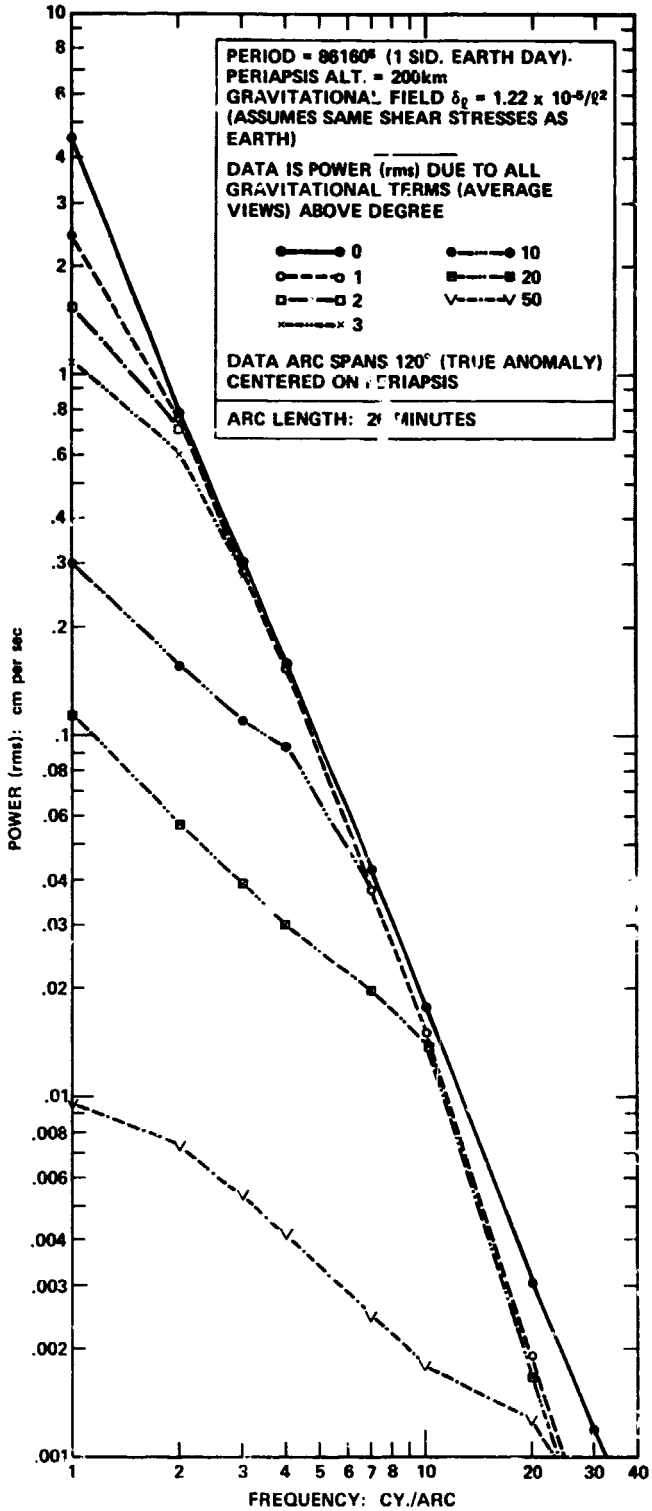

Figure 13a. Expected Power Spectrum in *LOS* Range Rate for a Pioneer Venus Orbiter

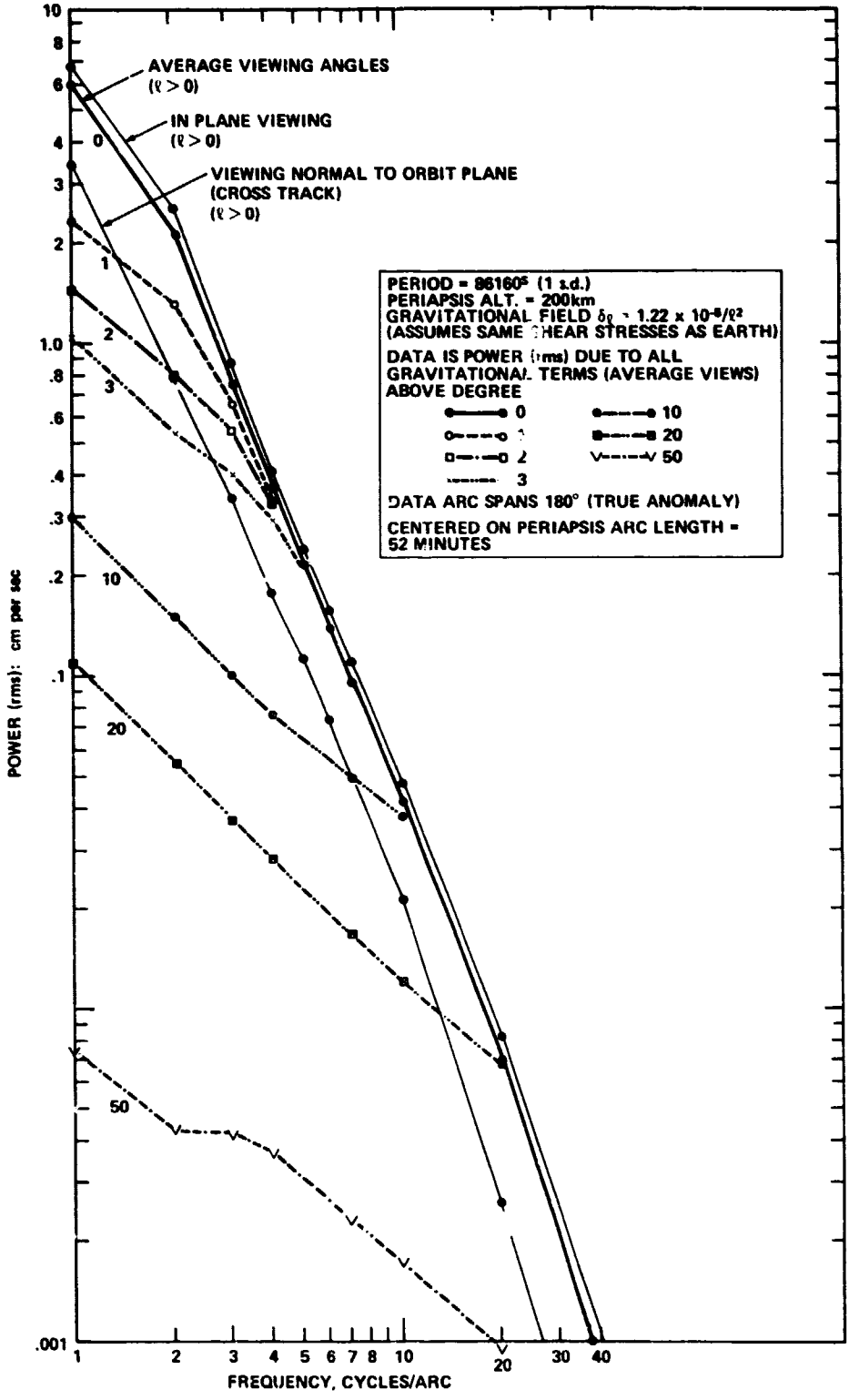

Figure 13b. Expected Power Spectrum in *LOS* Range Rate for a Pioneer Venus Orbiter

From Figure 13a, this is just at the signal level for 21 cycles. Reading across to lower frequencies at this level, this threshold power at 1 cycle is just affected by all the gravitational terms above about degree 55. The threshold power at higher frequencies are sensitive to only lower degree gravitational effects because the potential at altitude declines strongly with degree. Also, from Figures 13a and 13b, it is noted that appreciable power from low degree harmonics radiate to higher frequencies. But for the shorter data-arc at high frequency, this is due more to 'leakage' from the end discontinuity than the inherent power of the field.

THE EFFECT OF ORBIT DETERMINATION ON THE POWER SPECTRUM

The development of *LOS* perturbations here is to a fixed ellipse with mean elements which have not accommodated themselves to these fluctuations. But particularly when the tracking does not cover a full revolution or more, the determined reference orbit will necessarily adjust itself to the limited data thereby reducing the overall power of the gravitational fluctuations. In fact, tracking coverage is never sufficient; orbits always adjust to accommodate data.

If the mean orbit were known, the effect of orbit determination is merely the effect on the *LOS* of the variation between the adjusted and the true mean elements of the trajectory. This problem has been studied by Gottlieb (1970) in connection with the early direct use of *LOS* accelerations to model lunar Mascons (see also Phillips, et al., 1978). Since the problem arises from the difference of two ellipses, it can be expected that the greatest distortion (and reduction) will be in the lowest frequencies (0, 1 and 2 cycles/arc). On the other hand, if a good low order gravity model is used in the trajectory determination, this distorting effect of orbit error will be minimized.

An extreme example of *LOS* low frequency power reduction in orbit determination is shown in Figures 14 and 15. Figure 14 shows the ATS-6 to GEOS 3 *LOS* range rate signal from the Goddard Earth Model 6 (Smith, et al., 1976) less $\bar{C}_{20}$, on a 96 minute arc of an elliptic orbit before and after adjustment. The average *LOS* is inclined 60° to the orbit plane and, in spite of

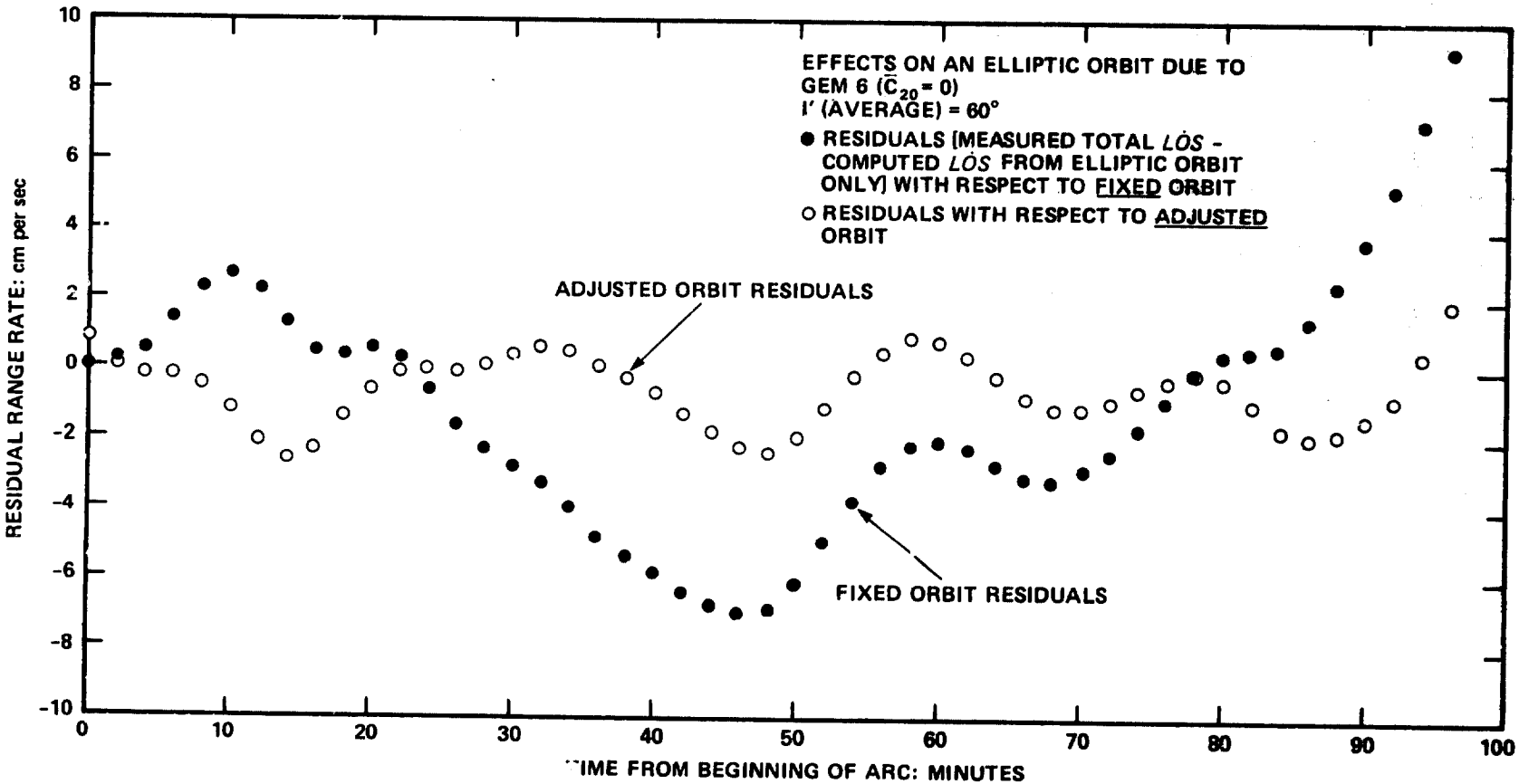

Figure 14. Simulated ATS-6/GEOS 3 Line of Sight Range Rate Residuals

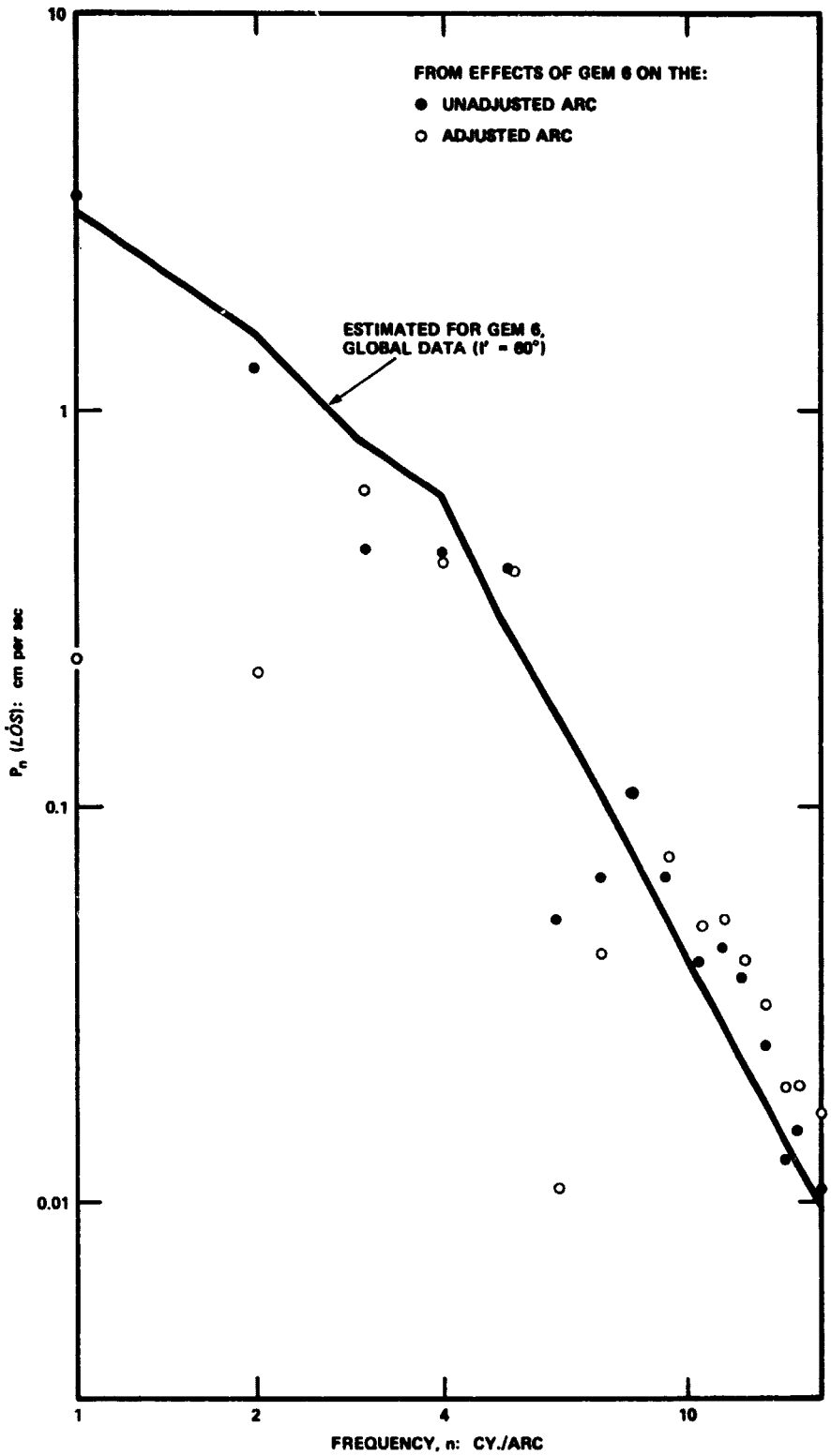

Figure 15. Power Spectrum for ATS-6/GEOS 3 Range Rate Residuals

the rather long arc, a large change of the orbit plane (mostly) is required in the orbit adjustment, eliminating most of the gravitational variation at 1 and 2 cycles. The end-matched power spectra for these two cases are shown in Figure 15 together with the predicted spectrum from GEM 6 (less $\bar{C}_{20}$). In fact, the power at all frequencies (to the beginning of 'leakage') for the unadjusted orbit is well predicted by the theory even though both planet and viewing aspects move. Here, Equation (15) was used for a full revolution of data. For the adjusted orbit, only the power at 0 (not shown), 1, 2 and 7 cycles is seriously deficient.

Another, less severe case is shown in Figures 16a,b. Figure 16a shows 40 minutes of *LOS* range rate residuals from ATS-6 to Apollo-Soyuz (rev. 115 over Africa) due to a field complete from (10,0) to (45,45). The geopotential was truncated from Rapp's (1977) model to illustrate the excellent predictions of the spectrum for high degree effects. The spectrum (Fig. 16b) is for the (simulated) residuals on an orbit adjusted to the signal. Evidently the accommodation is slight, to (mainly) high frequency fluctuations, because even the low frequency power is well predicted.

The simplest solution to the distortion of the residual tracking spectrum from orbit determination is just to ignore the low frequency residual power. As Figures 13a,b show, for the eccentric orbiter there should be enough power from low degree terms ($\ell \leq 3$) radiating to higher frequencies ($n > 2$) to maintain sensitivity for their solution. The solution for higher degree terms ($\ell > 3$) should be easier since they have maximum sensitivity at higher (undistorted) frequencies ($n > 3$).

A more sophisticated approach would be to solve directly from the tracking data for the orbit and point-mass concentrations along or near the track. The *LOS* accelerations of these on the orbit would yield an undistorted power spectrum. But, since the smoothed gravitational spectrum is all that is sought with limited data, it is probably sufficient for this purpose to ignore the lowest frequencies in the interpretation of the track spectrum even for circular orbits.

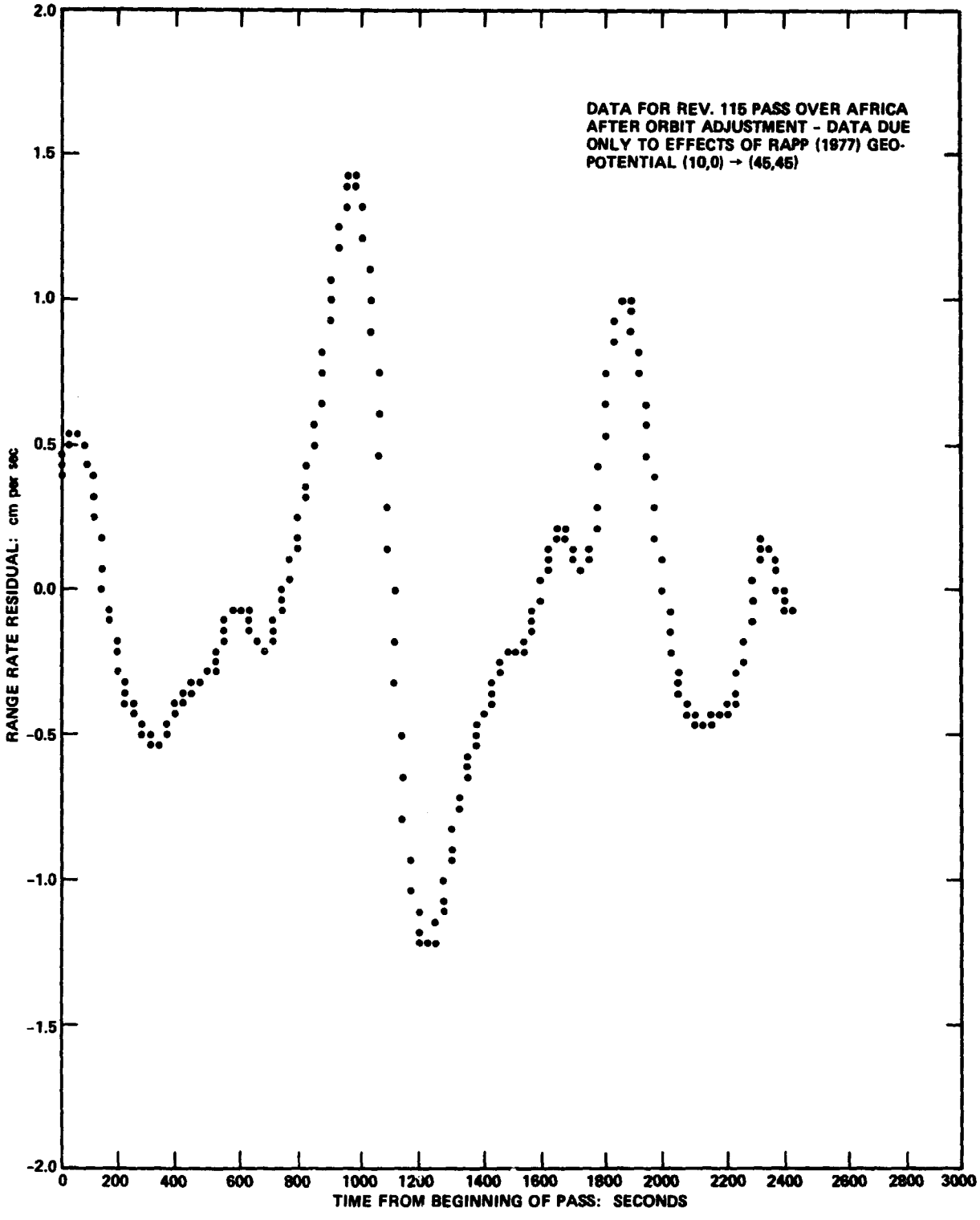

Figure 16a. Simulated ATS-6/Apollo-Soyuz Line of Sight Range Rate Residuals

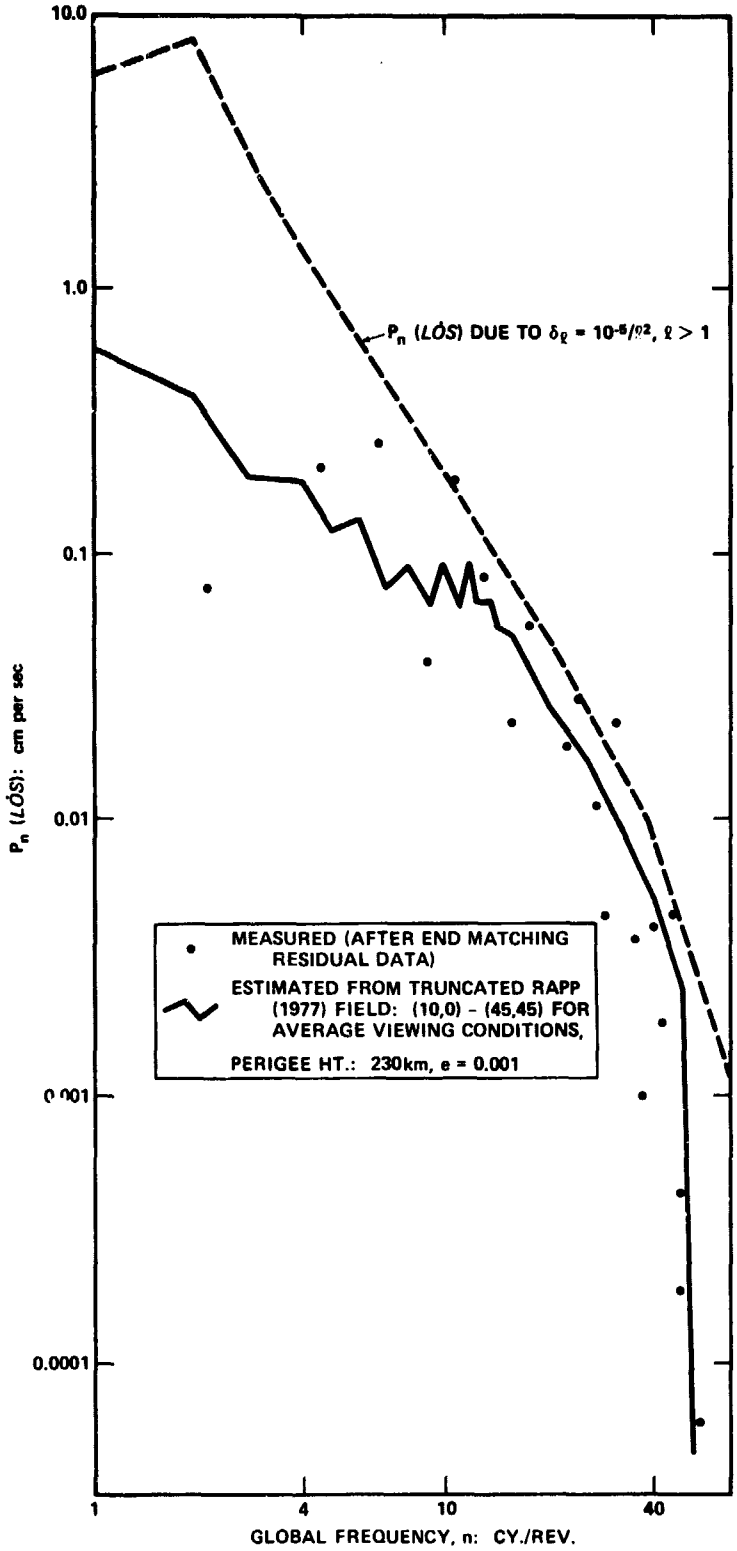

Figure 16b. Power Spectrum for Simulated ATS-6/Apollo-Soyuz Residuals

INVERSION OF TRACK POWER SPECTRA

The predicted *LOS* range rate tracking spectrum for an eccentric orbiter can be written as a linear transformation of the gravitational spectrum:

$$P_n^2(\dot{LOS}) = \sum_{\ell=0}^{\infty} S_{n,\ell}^2 \delta_{\ell-1}^2 \tag{27}$$

where $S_{n,\ell}^2$ are sensitivity coefficients calculable from Equations (12) and (26) for the appropriate orbit and viewing conditions. For the circular orbit case this system of equations generates two simple, uncoupled triangular matrices in $\delta_{\ell\ \text{even}}^2$ and $\delta_{\ell\ \text{odd}}^2$. There is no influence for $\ell < n$ in this case. Therefore, for circular orbits, given a measured track spectrum, the solution for the gravitational spectrum can proceed by simple back substitution in (27) starting at a sufficiently high degree and frequency. But for the eccentric orbit, the sensitivity matrix is full. Therefore, the solution for the gravitational spectrum, using (27), must proceed by inversion of ever larger (non symmetric) matrices until the result stabilizes.

A great simplification can also be accomplished in the eccentric orbit case if only a few parameters of a smooth gravitational spectrum is desired. Then Equation (27) can be formulated as a set of condition equations for each frequency of the track spectrum in terms of the smooth gravitational spectrum parameters.

For example, suppose we assume the smooth spectrum in the usual form:

$$\begin{aligned} \delta_\ell &= A\ell^B, \quad \ell > 0 \\ &= C, \quad \ell = 0 \end{aligned} \tag{28}$$

Equations (27) then become:

$$P_n^2 = C^2 S_{n,1}^2 + \sum_{\ell=2}^{\ell(\max)} S_{n,\ell}^2 A^2 (\ell - 1)^{2B}; \quad n = 1, 2, 3, \ldots . \tag{29}$$

which are non linear in 'A' and 'B.'

But these equations can be linearized about a 'starting' solution A_o, B_o, C_o. If the power at more than 3 frequencies are given, the equations can then be solved in a 'least squares' sense to minimize the squared residual $[P_n^2 \text{ (measured)} - P_n^2 (A, B, C)]^2$. Again, experimentation will be required to find whether the results are stable and the residuals smallest as the maximum degree considered becomes large.

The linearized condition equations for A, B and C are:

$$P_n^2 \text{ (measured)} = P_n^2(A_o, B_o, C_o) + \frac{\partial P_n^2}{\partial A_o} \Delta A + \frac{\partial P_n^2}{\partial B_o} \Delta B + \frac{\partial P_n^2}{\partial C_o} \Delta C, \qquad (30)$$

where:

$$\frac{\partial P_n^2}{\partial A_o} = 2A_o \sum_{\ell=2}^{\ell(max)} S_{n,\ell}^2 (\ell - 1)^{2B_o}$$

$$\frac{\partial P_n^2}{\partial B_o} = 2A_o^2 \sum_{\ell=2}^{\ell(max)} S_{n,\ell}^2 (\ell - 1)^{2B_o} \text{Log}_e(\ell - 1)$$

$$\frac{\partial P_n^2}{\partial C_o} = 2C_o S_{n,1}^2$$

and:

$$(A, B, C) = (A_o + \Delta A, B_o + \Delta B, C_o + \Delta C)$$

Of course, if the planets mass is well enough known 'C' can be set to zero. I retain it here because the Mascon model I use is not adjusted to give $\bar{C}_{oo} = 0$. Two great conveniences of the smooth spectrum equations are that:

(1) we can formulate them to suit the measurements, and

(2) we can edit or down weight those measurements which have known distortions, for example, due to 'leakage' at high frequencies, or orbit determination at low frequencies.

As an example of the numerical solution for a simple gravitational spectrum from a measured *LOS* power spectrum, I have analyzed 10 range rate arcs with respect to the (0,0) through (2,2)

model implied by the Mascon planet. The orbits for these arcs were all of high eccentricity, with only fair coverage over the planet and viewed from different aspects. Equations (17) and (26) were used to calculate the sensitivity coefficients and expected spectrum (Table 1). In the solution, only the measured power at n = 1, 2, 3 cycles per arc was used. Therefore, the solution for A, B and C [iteratively from (30)] was determined without residual error (starting from 10^{-5}, -2.0 and 10^{-5} respectively). The solution took 4 iterations to converge and the result is consistent with the discrepancy between the measured and predicted track spectrum; the measured being too high at low frequency and too low at high frequency.

INTERPRETATION OF *LOS* SPECTRUM: MARS-MARINER 9

The only planetary spacecraft in highly eccentric orbits for which suitably long arcs of tracking exist (prior to Pioneer Venus) are the Mars-Mariner and Viking orbiters (e.g., Gapcynski, et al., 1977; Sjogren, et al., 1975). The tracking of these orbiters has resolved gravitational features as small as 1200km (9th degree terms). These features show broad correlation with the topography of Mars. From this correlation, Ferrari (1977) has found that over large areas (low degree terms) the crust of Mars is significantly stronger (supports significantly higher loads) than that of the Earth. This finding can also be inferred indirectly from the low degree gravity spectrum of Mars which is significantly stronger than Kaula's scaled rule. (The assumption must be made, of course, that these terms arise from the crust.) It is of great interest to know whether the excess gravitational power holds for high degree terms as well because if it doesn't, Mars would have a relatively thinner less developed crust than the Earth. On the contrary, the powerful, broad topography of Mars argues for a relatively thicker, more developed (younger?) crust.

Published residual *LOS* tracking data (Gapcynski, et al., 1977, p. 4326) has been analyzed from a 194 minute Mars-Mariner 9 pass (rev. 354) over the Hellas Basin (Fig. 17). The range rate residual data from Gapcynski, et al., appears to show a significant high frequency signal. The residual measurements are referred to an orbit fit to the (one minute averaged) 2 way Doppler

Table 1

Spectrum and Sensitivities in Gravitational Recovery

LOS Track Spectrum (cm/sec)			Gravitational Spectrum δ_ℓ (10^{-6})				Spectral Sensitivities $S^2_{n,\ell}$: $a^y = a \cdot 10^y (cm/sec)^2$			
n	P_n (Expected) for Model	P_n (Measured) from Arcs	ℓ	Model (Actual)	Starting Solution	Converged Solution	$n/\ell \rightarrow$ $\downarrow$	1	2	3
1	1.580	1.871	0	7.99	10.00	11.02	1	1.91^{10}	2.33^{11}	1.40^{11}
2	0.511	0.391	1	2.19	10.00	2.23	2	9.21^{7}	2.19^{10}	1.32^{11}
			2	1.07	2.50	0.54				
3	0.161	0.113	3	0	–	–	3	3.02^{7}	9.62^{8}	1.70^{10}

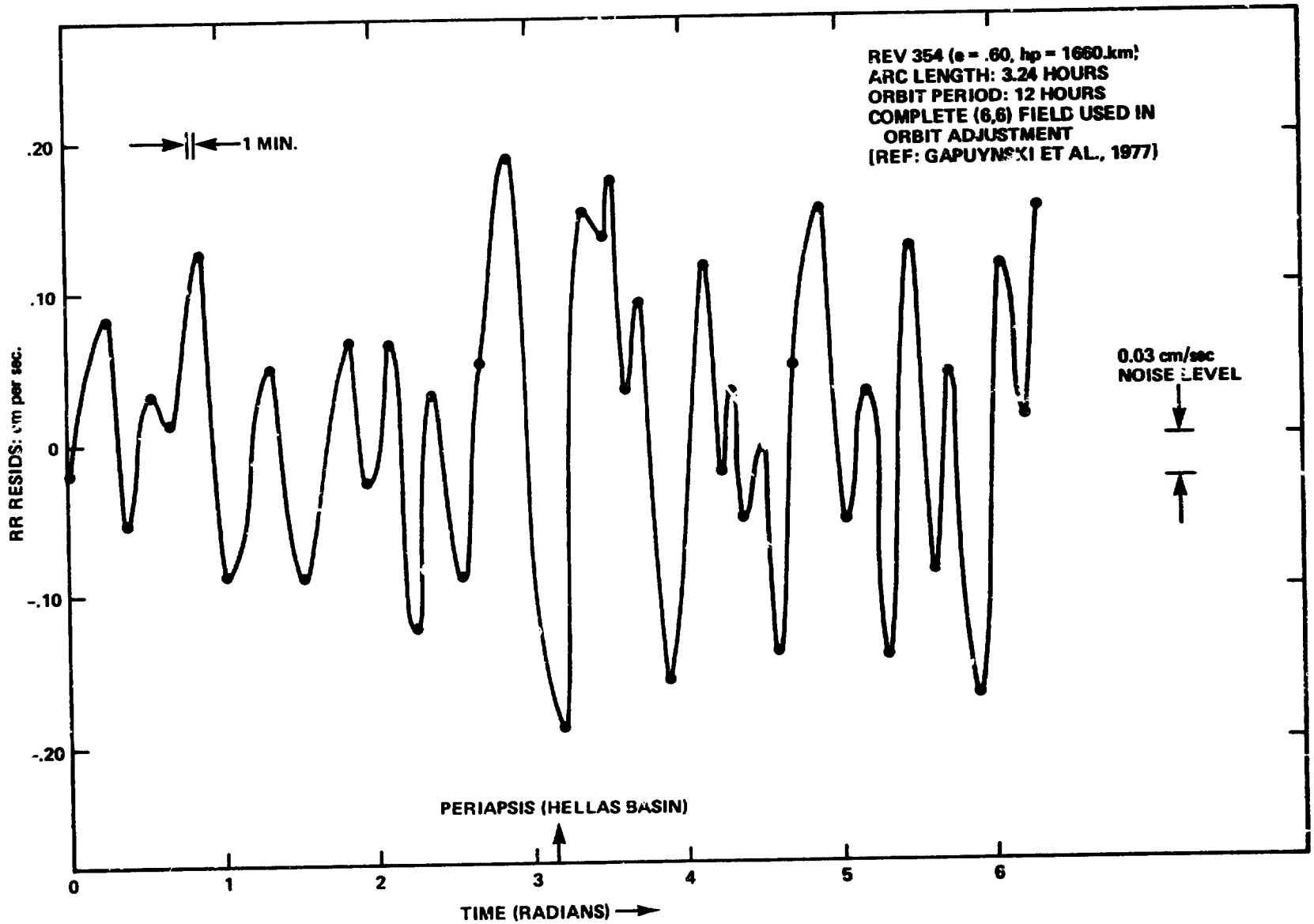

Figure 17. Range Rate Residuals: Mars Mariner (9)

signal with a complete 6th degree field. This field, in turn, used the tracking data in this pass so that we should expect to see the effects of aliasing in the residual power spectrum.

To achieve Figure 17, I hand-filtered the original residual points. From the original data the noise level appeared to be about 0.03 cm/sec. (I used 6.6 cm/sec/Hz to convert the S band Doppler (2300 MHz carrier) to range rate.) This seemed to be reasonable for 1 minute averaged data. Harmonic analysis was then performed on a 'signal' which was linear (a series of lines) between the turning points (highs and lows) of the filtered data. The harmonic noise characteristic of this filter was easily determined by averaging 10 analyses of the linear filter with random (σ = 0.03 cm/sec) data at the turning points. (Both signal and noise data were 'end matched' before being analyzed.)

The residual spectra of 'signal' and noise for this arc are shown in Figure 18 along with the expected spectrum for this orbit (e = 0.60, height of periapsis = 1660 km, average viewing conditions) from Kaula's scaled rule ($\ell > 6$). There are 3 parts to this figure, each important to the interpretation:

(1) The spectrum of the 'signal' (which includes an unknown amount of noise) declines from 1 to 6 cycles, then rises abruptly to a maximum at 9 cycles and generally declines after that, slowly to about 25 cycles then rapidly.

(2) The expected spectrum has a maximum at 1 cycle declining slowly to 7 cycles, then is almost flat to about 15 cycles where it precipitously loses almost all power. The flat portion is due to the 'sudden' introduction of gravitational power at $\ell > 6$. The rapid fall off at higher frequencies is due to the high altitude of the satellite.

(3) The estimated noise spectrum (shown for an overall level of 0.06 cm/sec) is flat to about 15 cycles falling steadily after that. Note that 42 turning points are involved, for a maximum estimation of about 21 frequencies if the data were equally spaced in time. The declining portion of both the noise and 'signal' spectra is clearly a characteristic of the

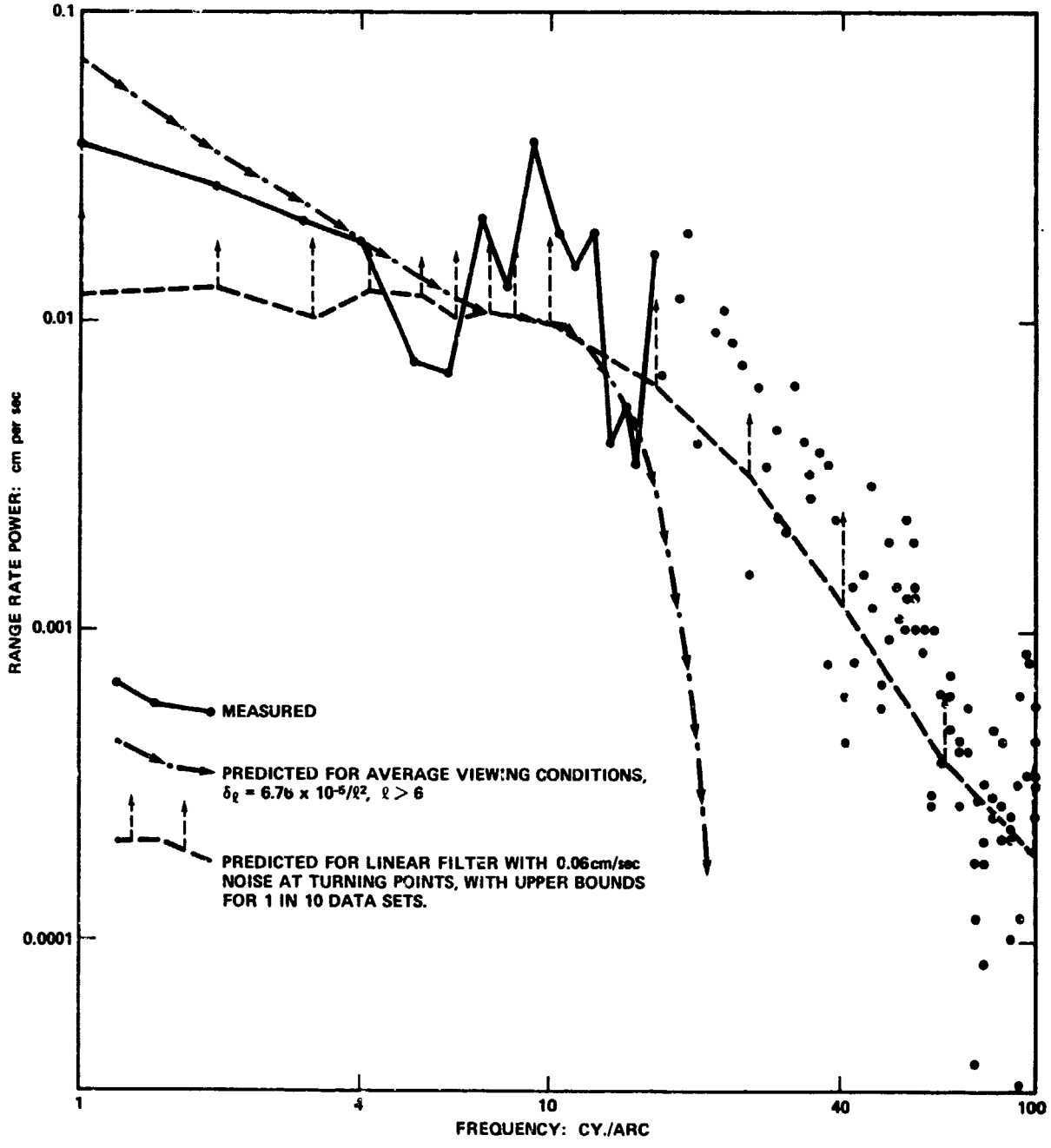

Figure 18. *LOS* Range Rate Residual Power Spectrum for Rev. 354, Mars Mariner 9

filter. The vertical arrows (in Fig. 14) give upper bounds (1 arc in 10) for the fluctuation of power among the 10 'random' noise data sets. Roughly speaking, 1 frequency out of 10 at an average random noise level of 0.06cm/sec will reach the power level at the end of the vertical arrows.

Clearly, the frequencies beyond 25 cycles are the result of noise which calibrates at some level above 0.06cm/sec. This result is somewhat surprising unless the data is sampled at, not averaged over 1 minute intervals (or is otherwise randomly disturbed). On the other side of the spectrum, the low end ($n < 6$ cycles) is just as clearly due to the gravitational spectrum above 6th degree of approximately the level as Kaula's scaled rule. The fact that the power at 1 cycle seems relatively low compared to the others may be the result of orbit adjustment to this data. The fact that this low frequency part of the signal is everywhere less than expected may be merely due to aliasing in the low degree gravitational harmonics fit to the Doppler tracking in this arc. The field solution has undoubtedly absorbed some of the low frequency information properly belonging to higher degree terms. Indeed it is more likely that the gravitational spectrum above degree 6 (for this arc) is stronger than Kaula's rule and the actual aliasing below 7 cycles is more severe still. This would permit the 'signal' highs at 9 and 19 cycles to be explained by the field at an average noise level only a little higher than 0.06cm/sec. For these features to be explained as noise would require a level of 0.09cm/sec which would virtually wipe out all of the apparently significant low frequency signal. In particular, the high at 9 cycles appears most likely to be a gravitational feature since it is the persisting fluctuation which reaches it's maximum effect at periapsis. As a confirmation of the above interpretation, I note that Sjogren, et al., (1975, p. 2899, 2900) report this data is indeed sampled (not averaged) at 1 per minute with an average noise level of 0.07cm/sec.

SUMMARY AND CONCLUSIONS

The line of sight track spectrum (accelerations and range rate) due to the gravitational field has been simply related to the source spectrum for general planetary orbiters under a variety of

viewing conditions. While the theory requires the line of sight orientation, the field and the orbit to be fixed during a pass, simulations under more relaxed conditions still show excellent results (see also Wagner and Colombo, 1978). The expected anomalous gravitational spectrum for the Pioneer–Venus orbiter has been worked out in detail for two cases of periapsis centered data. Harmonic terms as high as degree 55 may be visible in this data.

It appears likely that the power in the very lowest frequencies of the track spectrum will be reduced in the accommodation of the orbit to the data. This effect may either be estimated by mass modeling (or error analysis) or the low frequency terms may simply be ignored in the interpretation of the overall spectrum.

Interpretation of a residual track spectrum for a Mars-Mariner 9 pass over the Hellas Basin indicates gravitational features there stronger than Kaula's (equal–Earth–stress) rule for Mars.

ACKNOWLEDGMENTS

I thank Steven Klosko for the ATS–6/GEOS 3 simulations and helpful discussions. William Wells and Werner Kahn were instrumental in obtaining the data for the ATS–6/Apollo–Soyuz simulation. Oscar Colombo initiated this investigation by pointing out that the eccentric orbit case could not be obtained by a straightforward extension of the results for circular orbits.

REFERENCES

Allan, R. R., Resonance effects due to the longitude dependence of the gravitational field of a rotating primary, Planetary and Space Science, 15, p. 54, 1967a.

Allan, R. R., Satellite resonance with longitude dependent gravity–II, effects involving the eccentricity, Planetary and Sp. Sci., 15, 1829–1845; 1967b.

Allan, R. R., Depth of sources of gravity anomalies, Nature, Physical Science, 236, 22–23, 1972.

Ananda, M. P., Lunar gravity: a mass point model, J. Geophys. Res., 82, No. 20, p. 3063, 1977.

Ferrari, A. J., Lunar gravity, a harmonic analysis, J. Geophys. Res., 82, No. 20, 307, 1977.

Ferrari, A. J., An analysis of the spectral properties of the terrestrial, lunar and martian gravity fields, EOS, 58, No. 12, 1118, Dec., 1977.

Gapcynski, J. P., R. H. Tolson, and W. H. Michael, Jr., Mars gravity field: combined Viking and Mariner 9 results, J. Geophys. Res., 82, No. 28, p. 4325–4327, 1977.

Gottlieb, P., Estimation of local lunar gravity features, Radio Sci., 5, 301–312, 1970.

Guier, W. H. and R. R. Newton, The earth's gravity as deduced from the Doppler tracking of five satellites, J. Geophys. Res., 70, 4613–4626, 1965.

Heiskanen, W. and H. Moritz, Physical Geodesy, p. 31, W. H. Freeman and Co., San Francisco, Calif., 1967.

Hotine, M., Mathematical Geodesy, p. 180; U.S. Dept. of Commerce, Environmental Science Services Administration, Monograph No. 2; Washington, D.C., 1969.

Kaula, W. M., Theory of satellite geodesy, Blaisdell Pub. Co., Waltham, Mass., 1966.

Kaula, W. M., The gravitational field of the moon, Science, 166 (3913), 1581–1588, 1969.

Kaula, W. M., Geophysical inferences from statistical analyses of the gravity field, in: The Changing World of Geodetic Science, 1, 119–141, Ohio State University Dept. of Geodetic Science (Report 250), Columbus, Ohio, 1977.

Khan, M. A., Depth of sources of gravity anomalies, Geophys. J. Roy. Astrom. Soc., 197–209, 1977.

Lambeck, K., Lateral density anomalies in the upper mantle, J. Geophys. Res., 71, 6333-6340, 1976.

Phillips, R. J., W. L. Sjogren, E. A. Abbott, and S. H. Zisk, Simulation modeling to spacecraft-tracking data: analysis and application, J. Geophys. Res., 83, No. B11, 5455-5464, 1978.

Rapp, R. H., Potential coefficient determinations from 5° terrestrial gravity data, Ohio State Univ. Dept. of Geodetic Science, Report No. 251; Columbus, Ohio, 1977.

Sjogren, W. L., J. Lorell, L. Wong, and W. Downs, Mars gravity field based on a short arc technique, J. Geophys. Res., 80, No. 20, 2899-2908, 1975.

Smith, D. E., F. J. Lerch, J. G. Marsh, C. A. Wagner, R. Kolenkiewicz, and M. A. Khan, Contributions to the national geodetic satellite program by Goddard Space Flight Center, J. Geophys. Res., 81, No. 5, p. 1008, 1976.

Wagner, C. A., The accuracy of Goddard earth models, NASA-GSFC X-921-76-187, Appendix B; Greenbelt, Md., 1976.

Wagner, C. A., The spectrum of the geoid from altimeter data, NASA-GSFC X-921-77-63, p. 23; Greenbelt, Md. 1977.

Wagner, C. A. and O. L. Colombo, Gravitational spectra from direct measurements, NASA TM 79603, Goddard Space Flight Center, Greenbelt, Md., 1978.